

University of Nevada, Reno

**Thallium Isotope Implications for the Metalliferous Source of  
Carlin-type Deposits in northern Nevada**

A thesis submitted in partial fulfillment of the  
requirements for the degree of Master of Science in  
Geology from the University of Nevada, Reno

by

Katie Wickham

August, 2014



University of Nevada, Reno  
Statewide • Worldwide

THE GRADUATE SCHOOL

We recommend that the thesis  
prepared under our supervision by

**KATIE M. WICKHAM**

entitled

**Thallium Isotope Implications for the Metalliferous Source of Carlin-type Deposits  
in northern Nevada**

be accepted in partial fulfillment of the  
requirements for the degree of

**MASTER OF SCIENCE**

Greg Arehart, Advisor

John Muntean, Committee Member

Ben King, Graduate School Representative

Marsha H. Read, Ph. D., Dean, Graduate School

August, 2014

## Abstract

The Carlin-type deposits of northern Nevada comprise a world-class accumulation of Au deposits with a characteristic geochemical signature of elevated Tl, As, Hg, and Sb. Three possible sources of Au in Carlin-type systems have been described, and include: (1) leaching of Au from pre-enriched Paleozoic sedimentary rocks (2) metamorphic mobilization or leaching of Au from deeply-buried, metamorphosed late Proterozoic to early Cambrian clastic sedimentary rocks, and (3) magmatic-hydrothermal fluids evolved from magmas. Traditional geochemical and isotopic tracers, including Pb, H, O, S, and C, have yielded ambiguous results, and sources of hydrothermal fluids and their components, especially gold remain enigmatic.

Because there is a strong correlation between Tl and Au in these deposits, Tl can be considered as a proxy element of Au. This study describes the first-ever Tl isotope data collected for ore- and late-stage mineralization from a Carlin-type system, as well as for a suite of potential source rocks, with the goal of fingerprinting Au sources for these systems in northern Nevada. Although not pointing to an unequivocal origin for the Tl (and, therefore, Au), the Tl isotope data indicate that Paleozoic carbonate rocks are not a likely metal sources. In addition, comparison of ore- to late-stage minerals may suggest a shift in Tl isotope compositions that could be consistent with evolution of magmatic- and/or metamorphic-dominated fluid to a meteoric-dominated fluid with time.

## **Dedication**

To my family, whose love and undying support have carried me to great places.

## Acknowledgments

Thank you to Sune Nielsen and Jurek Blusztajn at the Woods Hole Oceanographic Institute for their collaboration in and out of the laboratory. Thanks to Greg Arehart for bringing me to UNR and introducing me to this project. Thanks to John Muntean for helping me see the bigger picture, and to John McCormack for always finding time to teach any student in need of learning, myself included.

## Table of Contents

1.	Introduction.....	1
	1.1 Carlin-type Disseminated Gold Deposits.....	1
	1.2 Thallium Isotopes.....	3
2.	Geologic Framework.....	6
	2.1 Brief Overview of Tectonic History of Northern Nevada.....	6
	2.2 Sample Description and Geologic Representations.....	9
	2.3 Characteristics of a Carlin-Type Deposit: Turquoise Ridge and the Getchell Trend.....	13
	2.4 Elemental Maps of Ore Sample from Turquoise Ridge.....	13
3.	Methods of Thallium Isotope Analyses.....	17
	3.1 Acid Digestions.....	17
	3.2 Liquid-Ion Exchange Chromatography.....	18
4.	Thallium Isotopic Data.....	20
5.	Discussion.....	20
	5.1 Geochemical Nature of Thallium.....	20
	5.2 Proposed Models of Metalliferous Sources for CTDs.....	22
	5.2.1 Sourcing Paleozoic Sedimentary Host Rocks.....	23
	5.2.2 Sourcing Metamorphosed Neoproterozoic Clastic Rocks.....	26
	5.2.3 Sourcing Magmatic Products,,,,,.....	27
	5.3 Ore- to Late-Stage Isotopic Shift.....	28
6.	Conclusion.....	29
7.	References.....	30

8. Appendix: Thin Section Characterization.....	38
---	----

## List of Tables

Table 1: Published thallium isotopic and concentration data for reservoirs.....	10
Table 2: Thallium isotopic and concentration data for study samples.....	18

## List of Figures

Fig. 1: Map of Sample Locations.....	1
Fig. 2: Time-Space Diagram Depicting Geologic History of Great Basin.....	7
Fig. 3: Schematic Cross Section of Great Basin Geology.....	9
Fig. 4: Simplified Geologic Map of the Getchell Trend and Schematic Cross Section of Turquoise Ridge.....	14
Fig. 5: Probe Image of Ore Pyrite and Elemental Maps of As, Au, and Tl.....	15
Fig. 6: Concentration Cross Sections of Tl and Au Across Ore Pyrite Grain.....	16
Fig. 7: Image of Liquid Ion Exchange Chromatography Columns.....	19
Fig. 8: Elemental Maps of Cu, K, and Tl Illustrating Geochemical Behavior in CTDs.....	21
Fig. 9: Thallium Isotope Plot of Sample Data.....	24

## 1. Introduction

### 1.1 Carlin-Type Disseminated Gold Deposits

Carlin-type deposits (CTDs) of northern Nevada (fig. 1) represent the second largest concentration of Au in the world and have made the U.S. the fourth largest producer of Au worldwide (Muntean et al., 2011). Four major trends, each made up of multiple deposits, comprise the majority of CTDs in northern Nevada and include the Carlin, Getchell, Battle Mountain-Eureka, and Jerritt Canyon trends (Muntean et al., 2011). Characteristics, such as association with igneous intrusions and isotopic data, can vary from trend to trend as well as from deposit to deposit, but some defining characteristics, such as structural control and geochemical signature, remain the same for all CTDs (Cline et al., 2005).



**Fig. 1** Map of sample locations (closed circles) and major trends of CTDs. Linear trends roughly follow geographic locations of deposits which comprise them.

Gold typically occurs in these systems as solid solution or submicron particles in arsenian pyrite which can either rim pre-existing pyrite grains (Wells and Mullens, 1973; Bakken et al., 1989; Archart et al., 1993) or occur as “fuzzy” micron-sized grains (Dobosz, 2010; Muntean et al., 2011). The distinct geochemical signature of CTDs is characterized by elevated Tl as well as As, Hg, Sb,  $\pm$ Te (Cline et al., 2005; Barker et al., 2009; Patterson and

Muntean 2011). Besides arsenian pyrite, ore-stage mineralogy includes quartz, illite, dickite, and kaolinite, while late ore-stage mineralogy includes quartz, calcite, pyrite/marcasite, realgar, orpiment, and stibnite (Cline et al., 2005).

Ore occurs as structurally and stratigraphically controlled replacement bodies that commonly root down to high-angle feeder faults where metalliferous ore fluids decarbonitized, as well as locally argillized and silicified, host units (Cline et al., 2005). Deposits commonly occur in the footwall of regional thrust faults which place less permeable, less reactive basinal silicic and basaltic units over contemporaneous host slope to shelfal facies carbonates (Cline et al., 2005). Decarbonitization and argillization of the carbonate units resulted in increased porosity and permeability, which drove increased fluid reaction and Au deposition primarily via sulfidation (Hofstra and Cline, 2000). Sulfidation was enabled by the presence of sedimentary pyrite in the host units, which provided a nucleation surface for arsenian pyrite deposition, and supported by the presence of reactive Fe, released by decarbonatization, in the host rocks (Stenger et al., 1998).

The fluid and metal sources for CTDs have remained enigmatic despite extensive research. Oxygen and deuterium isotope studies have indicated a meteoric source in most deposits (Archart, 1996; Emsbo et al., 2003), though data in the Getchell trend suggest a magmatic or metamorphic fluid source (Cline et al., 2005). Muntean et al. (2011) suggested that much of the data interpreted to be dominantly of meteoric origin permit a magmatic source that mixed extensively with meteoric water as fluid rose to the surface. Fluid inclusion studies reveal low deposition temperatures of approximately 180°-240°C and salinities of about 2-3% NaCl equivalent (Cline et al., 2005). Though some deposits are associated with coeval intrusive centers, many are not. Deposits are commonly associated with long-lived

high-angle fault zones that have been extensively reactivated (Muntean et al., 2007) The faults are interpreted to acted as conduits for upwelling hydrothermal fluids (Muntean et al., 2011; Pearson et al., 2008).

## 1.2 Thallium Isotopes

The application of thallium stable isotopes as a geochemical tool is relatively new and is the result of increased instrumental precision over the last two decades. The use of Tl stable isotopes as a cosmogeochemical tool was attempted several times between 1960 and 1994 using thermal ionization mass spectrometry (TIMS) but, due to the occurrence of mass discrimination inherent in the instrumentation, instrumental fractionation completely obscured the recovery of true fractionation values present in the samples (Nielsen & Rehkämper, 2011). In 1999, Rehkämper & Halliday outlined a technique which used multiple collector inductively coupled plasma mass spectrometry (MC-ICPMS) which produced errors one-third to one-quarter of those obtained using the TIMS method, making it possible to use thallium isotope measurements as a geochemical tracer.

Thallium isotope ratios are reported in epsilon ( $\epsilon$ ) units, which represent a one to ten thousand ratio and is calculated against a standard (eq. 1). The standard used for Tl isotopic system is NIST SRM 997, a high purity Tl metal (May and Watters, 2004). The use of  $\epsilon$  units is more convenient than  $\delta$  units, which represents a one to one thousand ratio, because of the relatively minor fractionation between stable isotopes of Tl, which is directly related to the minor mass difference between  $^{203}\text{Tl}$  and  $^{205}\text{Tl}$  compared to the overall mass of the isotopes (Nielsen & Rehkämper, 2011). This results in much smaller fractionation values compared to systems which use  $\delta$  notation, such as for O or S. Only two stable isotopes of

thallium occur naturally, which makes experimental determination of fractionation mechanisms difficult to empirically identify. However, with masses of 203 amu and 205 amu, mass-dependent fractionation alone should not be able to account for the difference of 35 ‰ units in thallium isotope ratios thus far observed on Earth (Nielsen & Rehkämper, 2011).

$$\varepsilon^{205Tl} = \left[ \frac{\left( \frac{^{205}Tl}{^{203}Tl} \right)_{Sample} - \left( \frac{^{205}Tl}{^{203}Tl} \right)_{Standard}}{\left( \frac{^{205}Tl}{^{203}Tl} \right)_{Standard}} \right] \times 1000 \quad \text{Eq. 1}$$

In papers published by Fuji et al. (1989), however, unusual fractionation of uranium isotopes during the enrichment process of  $^{235}\text{U}$  was described, and was later attributed to a parameter called nuclear field shift, a mass-independent parameter which involves nucleus size and electron density near the nucleus (Nielsen & Rehkämper, 2011). Nuclear field shift was originally accounted for in calculations that quantified stable isotope equilibrium reaction fractionation in terms of mass-dependent processes, but was considered a negligible factor (Bigeleisen and Mayer, 1947). After observations such as those made by Fuji et al. (1989), as well as mass-independent fractionation of O during the production of ozone (Hoefs, 1997), nuclear phase shift was reevaluated to understand how these effects could play an integral role in fractionation in some systems (Bigeleisen, 1996). Mass-dependent fractionation still contributes to thallium isotope fractionation and positively correlates with the effects of nuclear phase shift in Tl isotopes; the combination of these two processes result in fractionation large enough to make measurements and assess natural, fractionation-inducing processes (Schauble, 2007).

Fractionation of thallium in natural systems is process dependent, although the mechanisms causing fractionation have yet to be completely determined. Valence state is thought to play an important role in fractionation; it is believed that processes which oxidize Tl(I) to Tl(III) is the most likely mechanism to induce isotopic fractionation (Schauble, 2007). The highest known  $\epsilon^{205}\text{Tl}$  values (+10 to +14) are recorded from ferromanganese nodules where Tl is taken in from seawater (which has  $\epsilon^{205}\text{Tl}$  values between -8 and -5) as Tl(I) and oxidized to Tl(III) in oceanic sediments (Rehkämper et al., 2002). Low temperature (<150°C) hydrothermal alteration of oceanic crust is responsible for some of the lowest  $\epsilon^{205}\text{Tl}$  values known (as low as -16) with no strong evidence for redox changes in Tl. High temperature (~350-400°C) alteration of oceanic crust, in contrast, displays minimal fractionation with respect to MORB glass values, which fall around approximately -1.9 (Nielsen, 2006).

Since 1999, stable isotopes of thallium have been applied to geologic problems including estimating hydrothermal fluxes in oceanic crust (Nielsen et al., 2006) and providing evidence for the presence of oceanic sediment in hot spot volcanism, indicating oceanic crustal recycling (Nielsen & Rehkämper, 2011) among other applications. But until 2010, thallium isotopes had never been applied to hydrothermal ore-developing systems, despite the presence of elevated thallium in many deposit types. Baker et al. (2010) studied a Chilean porphyry copper deposit which included a discussion of thallium isotope variations between alteration types (propylitic, argillic, sericitic, potassic); although no clear overall isotopic zoning pattern was identified throughout the deposit. They noted Tl tended to act as a lithophile element in the porphyry system, following K, not S or Cu as might be expected for

Tl which was originally classified by Goldschmidt as being a chalcophile element (White, 2013).

This study has focused on Carlin-type disseminated Au deposits of Nevada, in which Tl correlates with Au. High concentrations of Tl and As also occur during late-stage mineralization, whereas Au concentrations are much lower during the late stage. In order to investigate the source of Au in CTDs, the Tl isotopic signature of ore-stage material was determined with the assumption that ore-stage Tl precipitated from the same metalliferous fluid as the Au. Thallium isotope ratios of samples representing potential source rocks for metals in CTDs and late-stage mineralization samples were also determined. These values were then compared to Tl isotope ratios of potential source rocks for Tl and Au for the CTDs in Nevada. An isotopic signature of late-stage mineralization was also determined to evaluate whether or not there was a significant shift in values from ore- to late-stage which might indicate a major change in the source of Tl in the collapsing hydrothermal system.

## **2. Geologic Framework**

### **2.1 Brief Overview of Tectonic History of Northern Nevada**

The geologic history of northern Nevada and the Great Basin is long and complex, but a basic understanding is critical to evaluating the potential sources of Tl, Au, and other components of the ore fluids that formed CTDs. The basement rocks underlying the Great Basin and comprising the lower crust originated as Paleoproterozoic terranes accreted onto the Laurentian craton (Cline et al., 2005). This package was rifted during the break-up of

Rodinia in the late Proterozoic, resulting in crustal scale rift faults zones. Sedimentation during this period led to the development of a westward thickening wedge of late Proterozoic and early Cambrian clastic rocks, which are now metamorphosed to greenschist facies (Dickinson, 2004). The deep-seated, high angle rift structures have been interpreted to have been reactivated periodically throughout the tectonic history of Nevada, ultimately focusing hydrothermal

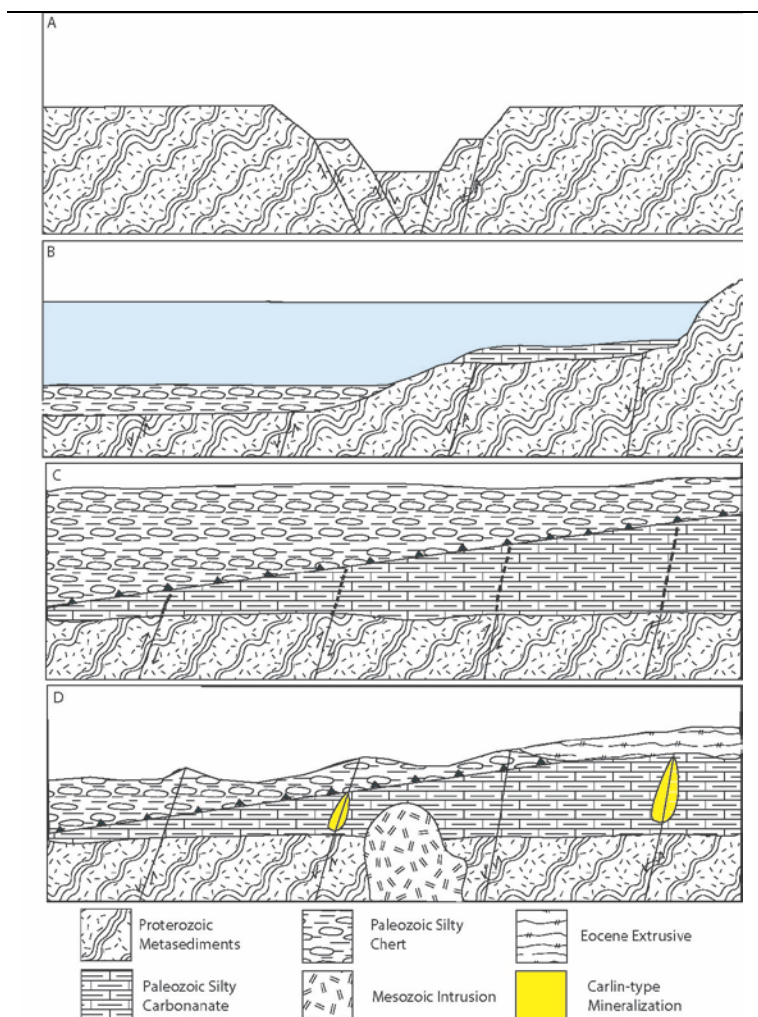


**Fig. 2** Simplified tectonic development of Nevada. (A) Proterozoic rifting generated basement-penetrating faults. (B) Passive margin sedimentation occurred during the Paleozoic. (C) Thrusting placed deep oceanic rocks over passive margin sediments during brief compressional orogenies, including the Antler orogeny responsible for the Roberts Mountains thrust fault. (D) Magmatism in the mid-late Mesozoic associated with Farallon subduction emplaced intrusions, and extension-related magmatism and Carlin-type mineralization occurred in the Eocene.

mineralization by acting as conduits for ore fluids (fig. 2a; Muntean et al., 2007).

Following active rifting, a passive margin environment allowed for deposition of mainly carbonate rocks from the early Paleozoic into the late Devonian (fig. 2b; Stewart, 1980). The passive margin sequence is characterized from east to west by shelf facies carbonates with lesser shales on the shelf, slope facies shaly to silty carbonates on the slope,

and cherts  $\pm$  basalt in the deep oceanic environment (Cline et al., 2005). Passive margin sediment accumulation ended at the onset of a compressional regime during the early development of the modern North American cordillera. Thrust faults were formed which placed deep oceanic silty cherts and basaltic rocks over the carbonate sequences (fig. 2c; Trexler et al., 2003); this compressional regime began with the Antler orogeny and emplacement of the Roberts Mountains thrust fault. The Antler orogeny, which lasted into the Mississippian, caused the formation of an eastward migrating foredeep basin in front of the thrust belt, where sedimentation occurred in through the Pennsylvanian (Cline et al., 2005). Extension and shortening in the Pennsylvanian and Permian was followed by thrusting related to the Sonoma orogeny in the early Triassic (Cline et al., 2005).

An active east-dipping subduction zone was established beneath North America in the mid Triassic, emplacing a magmatic arc just west of the Great Basin underneath the Sierra Nevada batholith (Dickinson, 2006). Back-arc magmatism was initiated underneath Nevada in the mid Jurassic through Cretaceous, observed today as intrusive bodies found throughout the Great Basin (fig 2d; Cline et. al, 2005). Shallowing of the subducting slab over time further added to compressional stresses acting on western North America and terminated magmatism in Nevada around 65 Ma (Humphreys, 1995; Cline et al., 2005); increased compressional stress had the effect of crustal over-thickening in the Great Basin (O'Driscoll et al., 2009; Coney and Harms, 1984).

In the Eocene, slab delamination, or rollback, caused (1) a sweep of renewed magmatism from northeast to southwest across Nevada (Humphreys, 1995) and (2) extension initiated in response to the over-thickened crust (Coney and Harms, 1984). This extension was, in part accommodated by the pre-existing basement-penetrating faults

(Muntean et al., 2011). Extension was of much higher magnitude in the Miocene after formation of the CTDs (fig. 2d; Seedorf, 1991).

## 2.2 Sample Description and Geologic Representations

To investigate potential models for the origin of metals in CTDs, we analyzed a suite of potential source rocks.

Though our analyses were limited in number, we choose samples representing the general categories comprising the geology of the Great Basin. Samples are qualitatively placed in the schematic cross section in figure 3.

Papoose 2 is a basalt sample from the Big Pine Volcanic Field near Bishop, CA. A sample from the Papoose Canyon Sequence was chosen due to its origins in the mantle underlying the Sierra

Nevada paleosubduction zone,

which we believe makes the Papoose basalt a good approximation for the mantle material

which supplied magmatism for Eocene volcanic activity in Nevada (Table 1). The Papoose

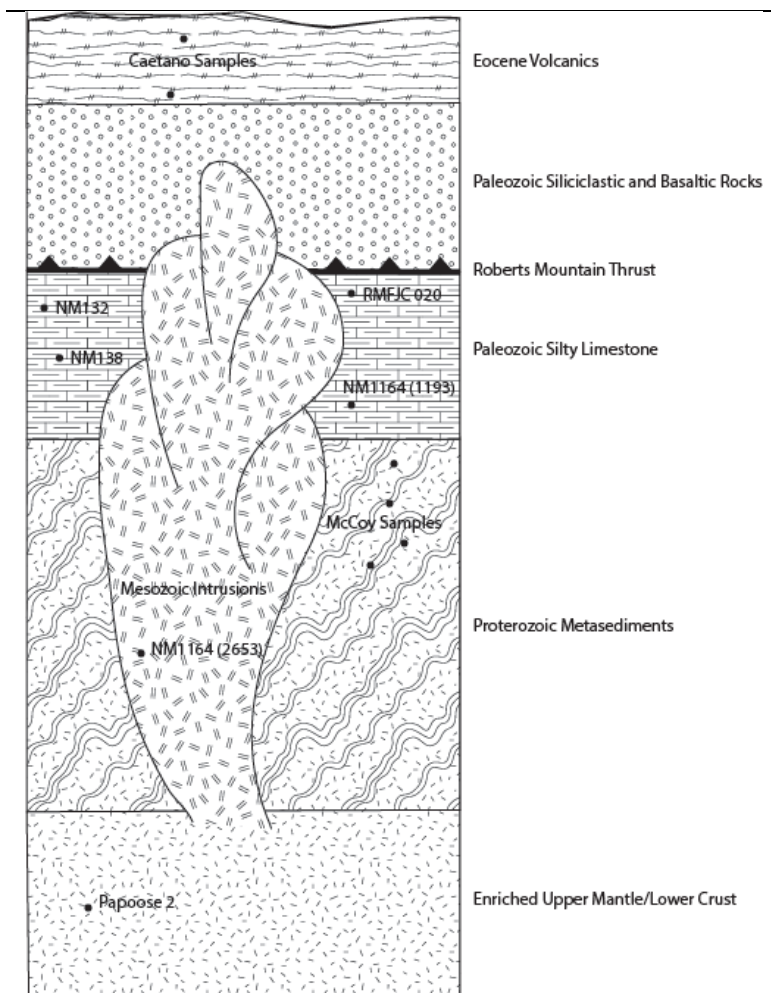


**Fig. 3** Schematic cross section depicting idealized Nevada stratigraphy with samples from this study qualitatively placed within.

Standard	Description	$\epsilon^{205}\text{Tl}$	Error ( $\pm$ )	[Tl] (ng/g)
Nod P1	Ferromanganese nodule	0.5	0.5	146 000
Nod A1	Ferromanganese nodule	10.7	0.5	108 000
AGV-2	Andesite	-3.0	0.6	269
BCR-2	Columbia river basalt	-2.5	0.4	257
BHVO-2	Hawaii basalt	-1.8	0.6	18
BIR-1	Iceland basalt	1.1	1.2	13
NASS-5	Seawater	-5.0	1.0	1.3
TSW	Coastal seawater, Tenerife	-8.7	1.0	0.0094
RRR	Rhine river water	-6.4	0.8	0.0036
Allende	Carbonaceous chondrite	-3.1	0.5	55

**Table 1** Published isotopic and concentration data for Tl in different standards. Modified from Nielsen & Rehkämper (2011).

Canyon sequence was characterized by Blondes et al. (2008) as a primitive (Mg # = 69) basalt. It is a young ( $760.8 \pm 22.8$  ka) volcanic product from a monogenetic basalt vent with highly forsteritic olivine phenocrysts, high and consistent Mg #s, and abundant mantle xenoliths indicate rapid ascent with little differentiation (Blondes et al., 2008).

Late Proterozoic metamorphic units, known as the McCoy Group, crop out at elevations of approximately 6,000-11,000 feet in the Schell Creek Range of northeastern Nevada. The McCoy sequence, which comprises metasediments from the Neoproterozoic to early Cambrian clastic wedge formed during the break up of Rodinia, was chosen for sampling because it is thought to be representative of the upper Proterozoic basement rocks underlying Nevada, and because of its low-grade, greenschist facies metamorphism (Misch and Hazzard, 1962). Samples were taken from the McCoy Creek Drainage (T. 18 N., R 66 E.), which is the type locality for the sequence, near Spring Valley, Nevada. Four samples of the McCoy Creek Group were analyzed and include two quartzites (McCoy 1 and McCoy 3)

and two phyllites (McCoy 4 and McCoy 5). McCoy 5 originally contained pyrite, though was significantly weathered and contained no remaining pyrite, only cubic iron oxide stained pits. We collected the 4 samples in an upsection transect through the drainage. As the total thickness of the sequence is in excess of 8,000 ft (Misch and Hazzard, 1962), 4 samples were analyzed to assess whether there is significant isotopic variation within the sequence.

Three drill core samples, NM1164(1193), NM132, and NM138, were collected from holes near the Turquoise Ridge deposit in the Getchell trend. Drill holes did not intersect Au mineralization (assay values <5 ppb Au), nor did the samples visually appear affected by hydrothermal alteration related to Carlin-type Au mineralization (ie. no argilization, silicification, or decarbonitization observed). All three samples were silty limestones, with some sparry calcite veinlets and minor amounts of pyrite. They are the same age and lithology as the rocks that host ore at Turquoise Ridge. Turquoise Ridge and the adjacent Getchell deposit were chosen for sampling because of recent extensive studies on the geologic framework and ore paragenesis (Chevillon et al., 2000; Cail and Cline, 2001; Cline, 2001; Cline et al., 2008, Muntean et al., 2009; Longo et al., 2009, Muntean et al., 2011) and is considered representative of a typical CTD.

We also sampled the Roberts Mountains Formation, a Paleozoic sedimentary unit in the lower plate of the Roberts Mountain Thrust, which hosts many CTDs in Nevada outside the Getchell trend. The sample (RMFJC020) is unaffected by hydrothermal alteration. It was collected from the Jerritt Canyon district of CTDs in Nevada several kilometers from known Carlin-type mineralization. Thin section petrography and reaction with weak HCl revealed the sample to be predominantly quartz silt set in a matrix of partially dolomitized calcite.

The Mesozoic intrusion sample, NM1164(2653), was taken from drill core about 2 km the Turquoise Ridge deposit. It is from a biotite-bearing granodiorite cogenetic with the 98 to 92 Ma Osgood Stock (Hall et al., 2000). This sample is thought to be representative of a typical Mesozoic intrusion found in the Great Basin and was chosen for its proximity to the Getchell deposit. Thin section petrography revealed minor alteration of feldspar to clay, minor chloritization of biotite, and intact hornblende indicating no hydrothermal alteration has affected the sample. The drill hole interval from which the sample collected assayed <5 ppb Au.

Two samples of Eocene rhyolitic ash flow tuffs (prefix “Caetano”) were collected from the Caetano Tuff, which was extruded from Caetano Caldera, the margin of which is a few kilometers south of the Cortez Hills CTD (John et al., 2008). The Caetano Tuff was chosen because it could be representative of the silicic magma underneath CTDs during the formation of these deposits (Ressel and Henry, 2006; Muntean et al., 2011). The Caetano Tuff has been extensively characterized (John et al., 2008) as a phenocryst-rich (approximately 30-55% by volume), welded rhyolitic ash flow tuff with >90% of phenocrysts being quartz, plagioclase, or sanidine with mafic mineral phenocrysts in minor abundance consisting of biotite or, rarely, amphibole. Thin section petrography showed minor differences between the two samples analyzed in this study; Caetano 2 contained minor amphibole while Caetano 1 did not, and Caetano 2 generally had smaller phenocrysts than Caetano 1.

Ore samples included a drill core sample (TU01166), which contained ore-stage arsenian pyrite which rims pre-ore pyrite. TU01166 is from the Turquoise Ridge deposit. The drill hole interval from which the sample was collected assayed 0.784 ounces/ton Au. A

sample (labeled “realgar”) precipitated from the late-stage(s) of the CTD hydrothermal system at the nearby Getchell deposit in the Getchell trend, was also selected from drill core for analysis. The core hole was from the 194 ore body. The drill interval from which the sample was collected assayed 0.326 ounces/ton Au. The sample was broken up with a hammer and realgar was hand-picked under a binocular microscope.

### 2.3 Characteristics of a Carlin-Type Deposit: Turquoise Ridge and the Getchell Trend

Several samples that were analyzed in this study were collected from the Getchell trend in northern Nevada (fig. 1) from either the Turquoise Ridge or the Getchell deposit. The Getchell fault is the central structural feature in the district (fig. 4) and strikes NNW dipping 40-55°E (Muntean et al., 2009). Ore-stage mineralization is hosted in strongly deformed Cambrian to Ordovician carbonate and clastic rocks with local, interlayered pillow basalts. Ore in the original Getchell deposit was originally mined from open pits along the Getchell fault (Chevillon et al., 2000). After the pits were mined out, mining of Getchell deposit moved underground into the footwall of the Getchell fault (Chevillon et al., 2000). Later the much larger Turquoise Ridge deposit was discovered in the hanging wall of the Getchell fault, and was put into production as an underground mine. As described above in other Carlin-type deposits, there is a main ore stage that results from dissolution and silicification of carbonate host rocks and argillization of silicates in clastic and basaltic host rocks. (Cail and Cline, 2001; Cassinerio and Muntean, 2011). Au-bearing arsenian pyrite, rich in Tl and other trace elements (Longo et al., 2009; Muntean et al., 2001) along with quartz,

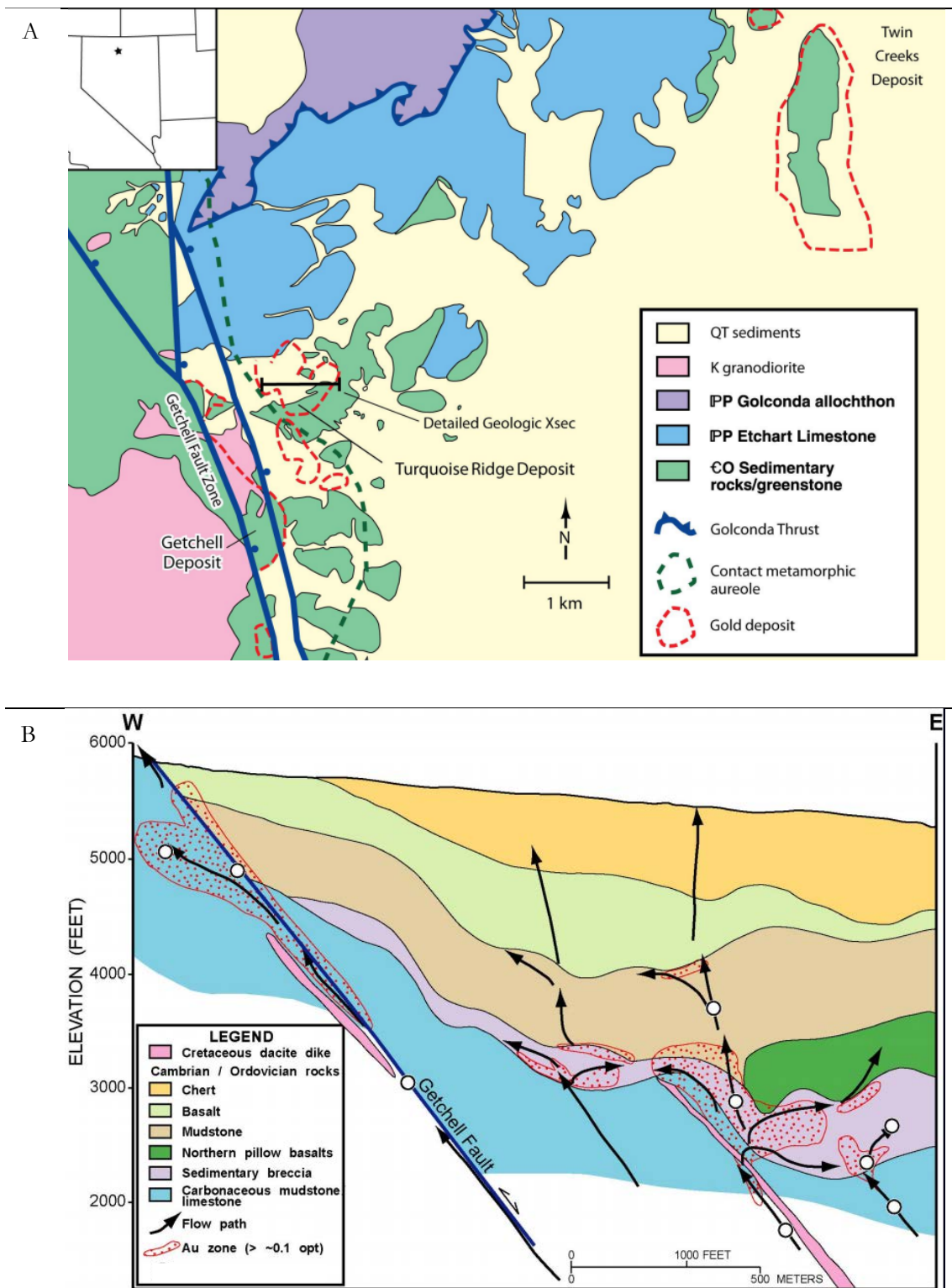
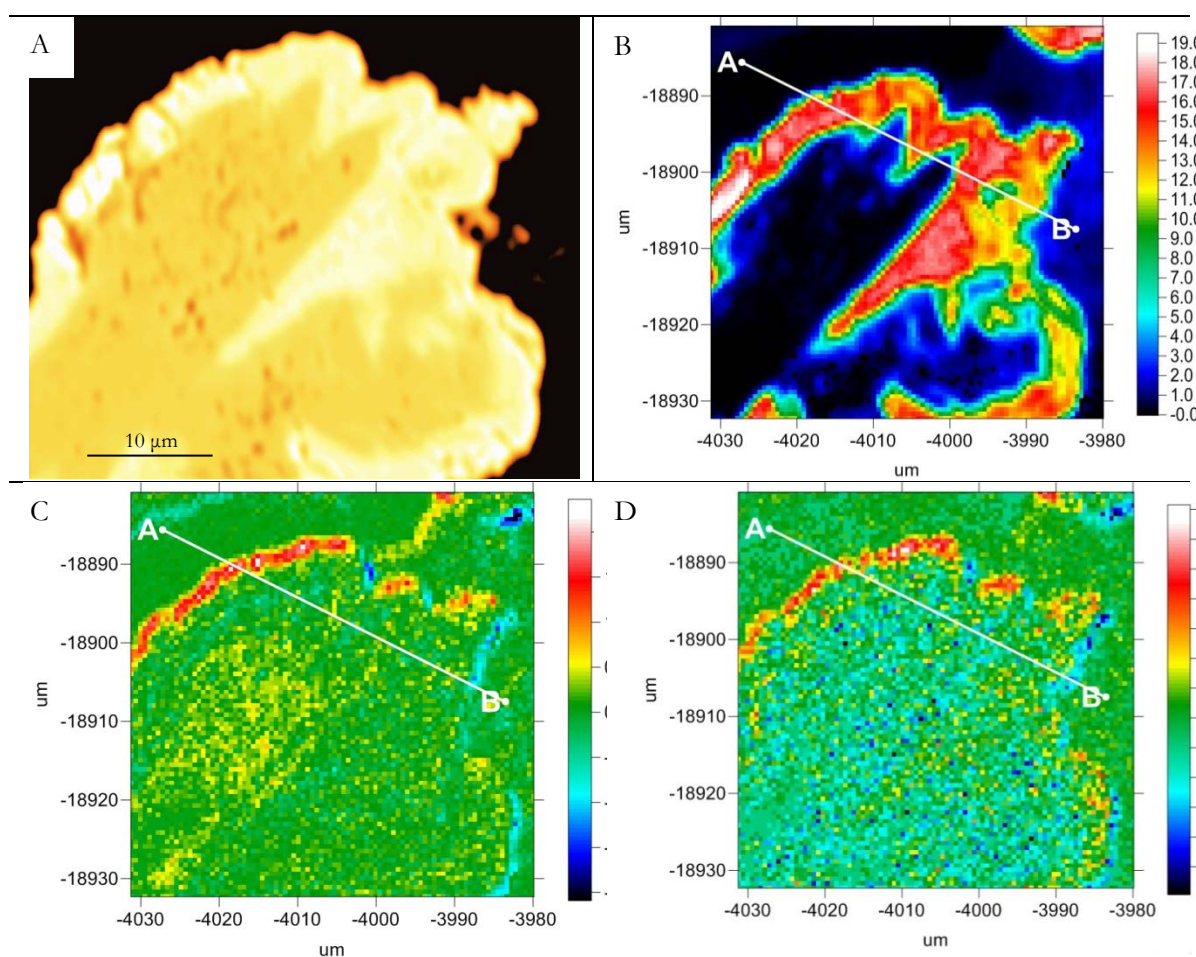


Fig. 4 (A) Simplified geologic map of a portion of the Getchell trend. (B) Schematic cross section of mineralization at the Turquoise Ridge deposit. Modified from Cline et al. (2008)

illite, and kaolinite formed during this main stage. With collapse of the hydrothermal system, realgar, orpiment, galkhaite a Tl-bearing sulfosalt), alcite and other minerals formed in the late stage, during which minor gold mineralization occurred (Cline, 2001).

#### 2.4 Elemental Maps of Ore Sample from Turquoise Ridge

In order to assess whether the Tl occurred with Au in the ore-stage pyrite from the sample of ore from Turquoise Ridge (sample TU01166), elemental x-ray mapping was performed using an Electron Microprobe Analyzer (EMPA) at the University of Oregon. A



**Fig. 5** EMPA elemental maps and concentration transects through the pyrite grain seen in (A) from the ore sample, TU01166. Maps show concentrations of (B) As, (C) Au, and (D) Tl. All concentrations in weight %. Shows excellent correlation of Tl and Au in As-rich rims around pre-ore pyrite, see fig. 6 for elemental abundances along cross section line shown in (C) and (D).

Cameca SX-100 EMPA was utilized for high precision data acquisition. Matrix correction was done using a pyrite standard in which trace elements of interest for the ore stage sample were assumed to be zero. This allowed for detection limits of Tl and Au low enough for elemental mapping. In addition, Tl point analyses giving concentration data for pre-ore and ore-stage pyrite were performed to determine the validity of assuming the Tl isotopic signature of the bulk sample represented the ore material and that no significant contribution of Tl came from pre-ore material. The maps (fig. 5) show high Tl concentrations in

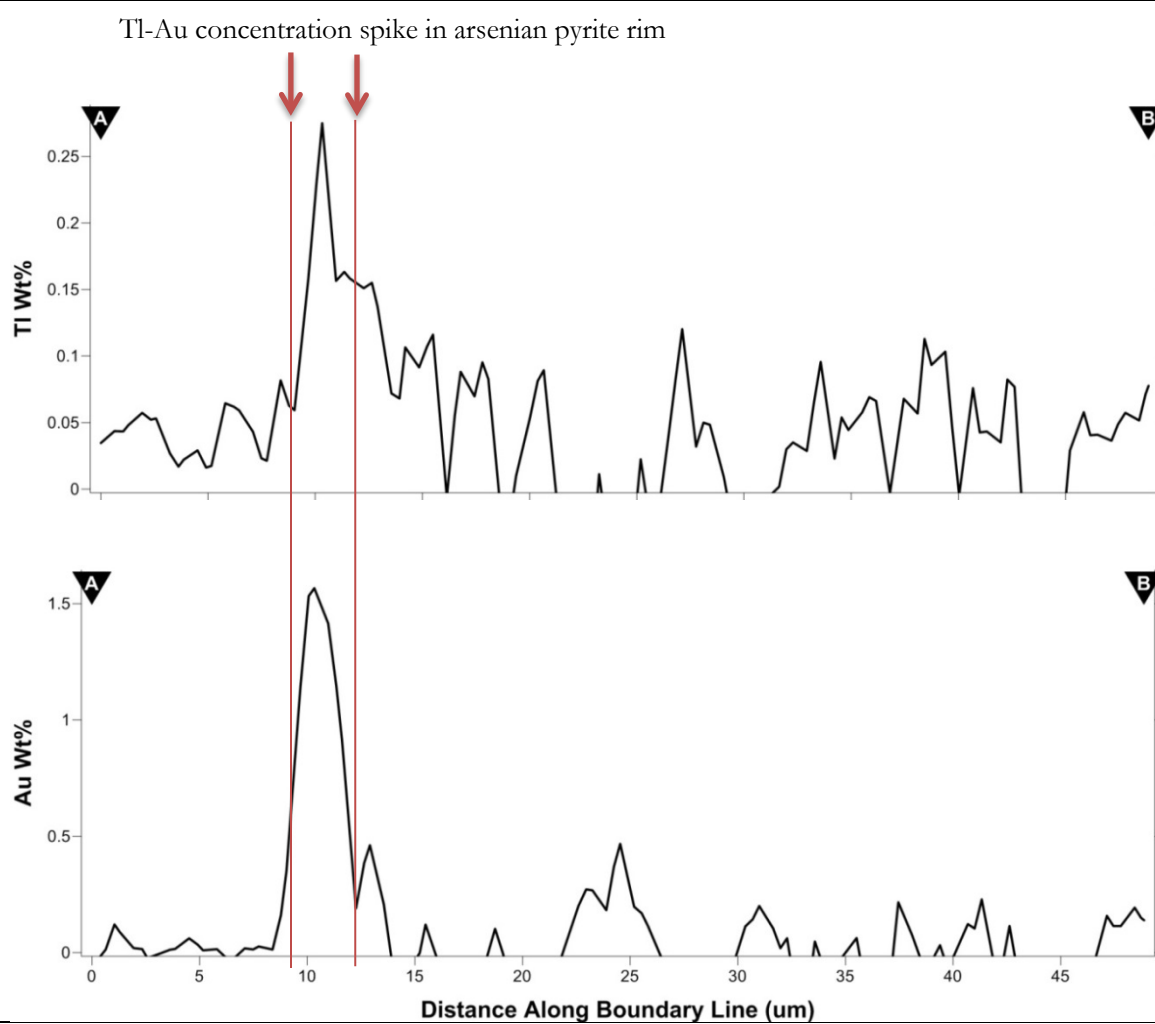


**Fig. 6** Transect through arsenian pyrite rimmed pyrite grain from ore-stage sample (TU01166). Shows a correlation of elevated concentrations of Au and Tl. Also shows the low abundance of Tl in pre-ore pyrite cores (BDL). For location of transect line, see fig. 5.

approximately the same location within the grains where high Au concentrations are found. Low resolution of the data is due to increasing sampling time at the expense of pixel size, which was necessary to detect low concentrations (100-200 ppm) of the trace elements in the grains. In addition, maps, as well as spot analyses performed on many grains, showed no significant enrichment of Tl occurred in pre-ore (low As) pyrite cores (fig. 6).

### **3. Methods of Thallium Isotope Analyses**

The determination of thallium isotope ratios was performed at the Woods Hole Oceanographic Institute using multiple collector inductively coupled plasma mass spectrometry (MC-ICPMS). Samples were prepared for MC-ICPMS analyses by liquid-ion exchange chromatography after multiple acid digestions utilizing hydrofluoric, nitric, and hydrochloric acids. A detailed description of processes involved in preparation and analyses for Tl stable isotope compositions is outlined by Rehkämper and Halliday (1999). Before Tl analyses were performed, samples were pulverized and analyzed via ICP-MS for Tl concentrations (table 2) by ALS Minerals. Most samples (with the exception of the Realgar sample, which had sufficiently high Tl concentrations) were analyzed against a standard specifically for low-level Tl.

#### **3.1 Acid Digestions**

Sample splits were taken from pulverized samples and weighed to give final thallium content of about 20 nanograms per sample split with some variation (up to 102 nanograms and down to 13 nanograms). Some samples had two splits weighed for analysis, which we

refer to as duplicate samples. The sample splits were immersed in hydrofluoric and nitric acids in sealed Teflon beakers and placed on a hot plate at approximately 125°C overnight. The caps were then removed from the beakers and the acid was allowed to evaporate silica tetrafluoride vapors as well as residual acid. The sample splits were subsequently treated with nitric and hydrochloric acids and subjected to sonication in order to remove any remaining fluorine bound as halides to cations. Evaporation of nitric and hydrochloric acids and acid treatments were repeated cyclically to ensure complete fluorine removal. Concentrated hydrochloric acid was then added to sample splits to remove residual nitrate. Concentrated

Category	Sample ID	$\epsilon^{205}\text{Tl}$	$^1\text{Error}$	$^2n$	[Tl] (ng/g)
Mantle-Analogous Basalt	Papoose 2	-1.13	$\pm 0.24$	2	70
Proterozoic Clastic Metasediments	McCoy 1	-1.44	--	1	150
Proterozoic Clastic Metasediments	McCoy 3	-1.58	--	1	90
Proterozoic Clastic Metasediments	McCoy 4	-1.54	$\pm 0.24$	2	740
Proterozoic Clastic Metasediments	McCoy 5	-2.41	$\pm 0.13$	2	500
Paleozoic Carbonate Lower Plate	NM 138	-2.72	--	1	420
Paleozoic Carbonate Lower Plate	NM 132	-3.28	$\pm 0.11$	2	390
Paleozoic Carbonate Lower Plate	NM 1164 (1193)	-4.28	--	1	400
Paleozoic Siliciclastic Lower Plate	RMFJC 020	-2.07	--	1	360
Cretaceous Granodiorite Intrusive	NM 1164 (2653)	-2.33	$\pm 0.11$	2	460
Eocene Rhyolitic Tuff	Caetano 1	-1.95	--	1	610
Eocene Rhyolitic Tuff	Caetano 2	-2.10	$\pm 0.05$	2	710
Ore-Stage Pyritic Ore	TU1166	-1.28	$\pm 0.10$	2	8400
Late Stage Realgar	Realgar	-2.11	$\pm 0.13$	2	127000

**Table 2** Tl concentration and isotopic data for ore-related minerals and potential source rocks.  $^1\text{Error}$  was calculated as the deviation from the mean of two sample splits, however, analytical error for all samples is assumed to be approximately 0.3.  $^2n$  is the number of sample splits analyzed.

hydrochloric acid was allowed to evaporate off and the sample splits were then redissolved in 1M hydrochloric acid for liquid-ion exchange chromatography.

### 3.2 Liquid-Ion Exchange Chromatography

Prior to the process of liquid-ion exchange chromatography, 5% bromine saturated

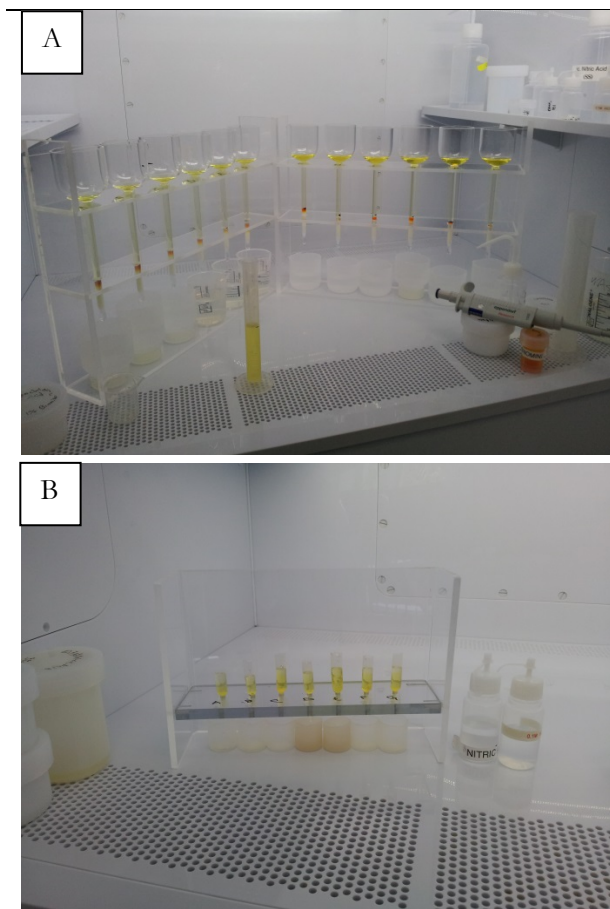


**Fig. 7** Liquid-ion exchange chromatography columns used to extract Tl from digested rock. (A) Primary columns and (B) secondary microcolumns.

water was added to the 1M hydrochloric acid to maintain an oxidizing environment which would ensure conversion of Tl(I), the thermodynamically stable valence state of aqueous thallium at standard pressure and temperature, to Tl(III). The change in valence state ensured complete chlorine complexing of aqueous thallium in the solution and retention by the inorganic resin used to filter the sample.

The resin (AGI x 8) is an inorganic material with extreme affinity for Tl(III). The thallium chloride-containing solution was allowed to

percolate through the resin placed in the tips of liquid-ion exchange chromatography columns (fig. 7a); the resin bonded to the thallium chloride complex allowing other elements to pass through to a waste container. After rinsing with oxidized solution to ensure removal

of all elements except Tl and Cl, the resin was then subjected to reducing solutions which allowed for the conversion of Tl(III) adhered to the resin back to Tl(I), which liberated the Tl from the resin. The aqueous Tl was collected in beakers and the process was repeated in micro-columns (fig. 7b) for further purification. The final sample Tl was suspended in a mass spectrometer solution, a mixture of 0.1 M HNO<sub>3</sub> and 0.1% H<sub>2</sub>SO<sub>4</sub>, and analyzed via MC-ICPMS.

#### 4. Tl Isotopic Data

Tl isotopic data (summarized in table 2) were collected from the suite of rocks described above. Mean values are reported for samples from which two sample splits were analyzed. Error values in table 2 represent deviation of sample split values from the mean value for the sample. The analytical error inherent in instrumentation is thought to be approximately  $\pm 0.3$   $\epsilon$  units for all samples.

The realgar sample is representative of late-stage mineralization in the Getchell trend ore system and yielded a value of  $-2.11 \pm 0.13$ . The sample of the main ore-stage at Turquoise Ridge had an  $\epsilon$  value of  $-1.28 \pm 0.10$ . Neoproterozoic clastic wedge and mantle-derived basalt samples ranged from  $-0.89$  to  $-1.77$ , with the exception of sample McCoy 5 which was significantly lower at  $-2.41 \pm 0.13$ . The isotopically lightest samples were from the Paleozoic carbonates which ranged from  $-2.72$  to  $-4.28$ . The Paleozoic dolomitic siltstone (sample RMFJC 020) was heavier at  $-2.07$ . Two samples of Caetano tuff were  $-1.95$  to  $-2.14$ , while the Mesozoic intrusion sample was slightly lighter at  $-2.33 \pm 0.11$ .

## 5. Discussion

### 5.1 Geochemical Nature of Thallium

Though originally classified by Goldschmidt as a chalcophile element (White, 2013), Tl occurs in most natural systems as  $Tl^+$  behaving geochemically similar to the lithophile elements, in particular following  $K^+$  and  $Rb^+$  (Nriagu, 1998). In CTDs, however, we believe that Tl behaves as a chalcophile element, substituting for S in pyrite. Evidence for chalcophilic behavior can be observed in EMPA elemental maps, as described above, of Tl, Cu, and K (fig. 8) where a clear correlation is seen between Tl and the chalcophile element Cu and no correlation exists between Tl and the lithophile element K. For the non-mineralized samples analyzed in this, we expect Tl to substitute for K.

Thallium isotopes were utilized in this study for two reasons: (1) the excellent correlation of Tl and Au (Cail and Cline, 2001) in CTDs suggesting deposition from a common fluid, and (2) the fact that, outside of rare, extremely oxidizing,

environments which may convert Tl(I) to Tl(III), Tl isotopic ratios are preserved through

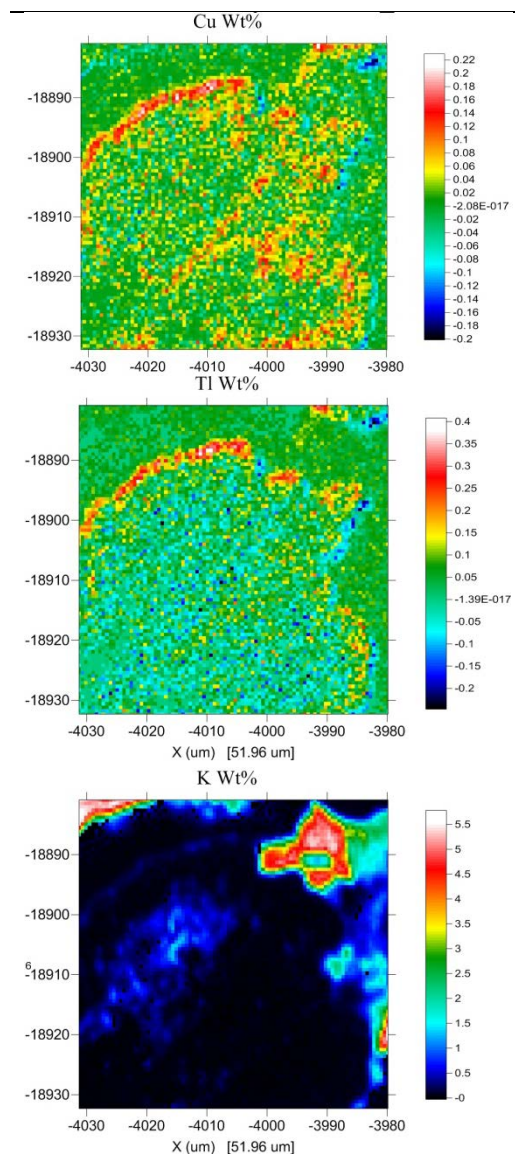


**Fig. 8** EMPA elemental map of pyritic ore shows excellent correlation of Tl and Cu and no good correlation between Tl and K. This indicates that Tl behaves chalcophilically in CTDs.

most processes (Nielsen & Rehkämper, 2011). Because Tl is rare in nature, and because it is elevated in CTDs, the isotopic signature of CTD ore should preserve the signature of the Tl, and presumably Au, source.

One natural process is known to fractionate Tl significantly, which is the oxidation of aqueous Tl in seawater during the formation of ferromanganese nodules (Rehkämper et al., 2002). Because one isotope is preferred for oxidation, fractionation occurs, causing very heavy isotopic values in ferromanganese nodules (+10 to +14) and leaving seawater significantly lighter (-5.5 to -6.0) than average crustal values (-2.0) (Rehkämper et al., 2002; Nielsen & Rehkämper, 2011). Since oceanic reservoirs are lighter, sediments precipitated directly out of seawater are expected to be significantly lighter than igneous sources or sediments accumulated due to crustal weathering (siliciclastic), which is observed in the data from Paleozoic carbonate rocks. The exception to this is if seawater sediments contain ferromanganese nodules, in which case isotopic values would be expected to be much heavier than crustal values.

## 5.2 Proposed Models of Metalliferous Sources for CTDs

Three general models calling for different metal sources have been outlined in the literature and include: (1) a local, metal-enriched, sedimentary source (Large et al. 2011; Emsbo et al., 2003), (2) a source from metasedimentary rocks (Ilchik and Barton, 1997; Seedorf, 1991), and (3) a magmatic, mantle-derived source (Muntean et al., 2011). Each model in the literature proposes an ore fluid responsible for moving metals from the source. Proposed ore fluids include (1) meteoric, (2) metamorphic, and (3) magmatic fluids. It is difficult to separate discussions of source of metals from those of the ore fluids; however, as

Tl isotopic data will only give us insight into source rocks, and not transport fluids, it is important to make the distinction.

Oxygen, hydrogen, and sulfur isotopic data differ between CTDs and are not solely diagnostic of one model. For instance, the Getchell deposit has produced oxygen and deuterium isotopic data, particularly isotopically heavy hydrogen, which indicates a contribution from magmatic or metamorphic water to the ore fluid (Cline and Hofstra, 2000), while many other CTDs, such as those of the southern Carlin trend, have values which indicate precipitation from predominantly evolved meteoric fluid (Cline et al., 2005, Arehart, 1996). Sulfur isotopic data also suggest potentially different sources of sulfur in different deposits. For instance at the Betze-Post-Screamer deposit ( $\delta^{34}\text{S}$  about -1 to +4‰, though one value was 7‰; Kesler et al., 2005), a magmatic sulfur source is suggested, whereas as a sedimentary source is suggested from the Meikle deposit, as indicated by heavy sulfur values ( $\delta^{34}\text{S}$  about 7 to 13‰; Emsbo et al., 2003). In the past, isotopically heavy sulfur was considered strong evidence of derivation by leaching of sedimentary upper crustal rocks (Arehart et al., 1996). However, some plutons in the Great Basin have been recorded to contain anomalously high  $\delta^{34}\text{S}$  (+20‰), values atypical of igneous rocks (Arehart et al., 2013), suggesting fluids with heavy sulfur could be sourced from magmas. Oxygen and deuterium isotope data, similarly, can be interpreted to reflect mixing of small amounts of deep metamorphic or magmatic waters, containing isotopically heavy hydrogen, with large amounts of evolved meteoric water, containing isotopically light hydrogen, during fluid ascent (Cline et al., 2005; Muntean et al., 2011). We present some models for genesis of Carlin-type deposits in the following sections for the purpose of discussing viability given our isotopic data which are plotted in figure 9.

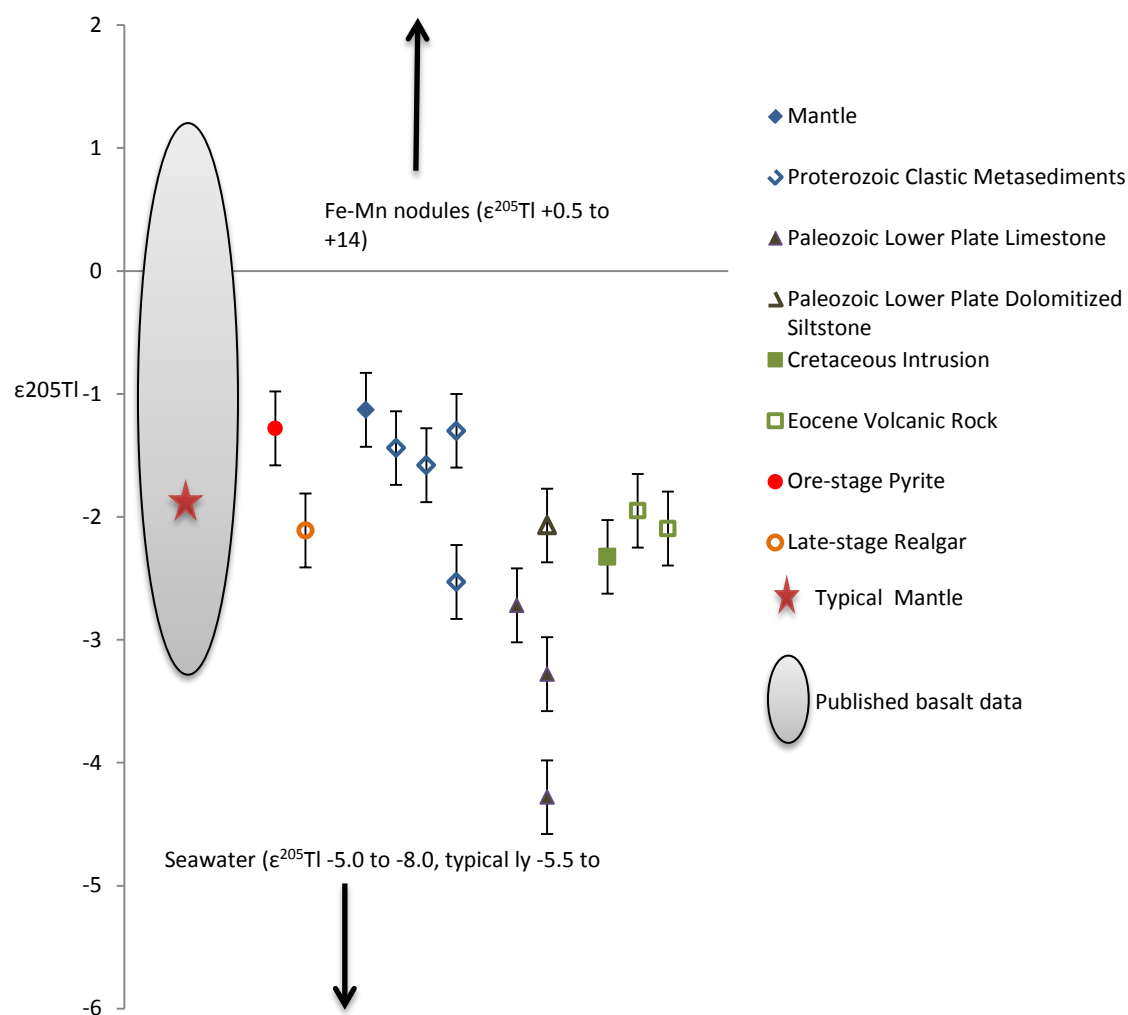


**Fig. 9** Average  $\epsilon^{205}\text{Tl}$  values for samples representing an idealized stratigraphy of Nevada as well as late- and ore- stage minerals from Turquoise Ridge in the Getchell Trend, a Carlin-type deposit in northern Nevada. Basalt, seawater, and ferromanganese nodules data from Nielsen & Rehkämper (2011). \*Note that error bars are uniformly  $\pm 0.3$ , not error calculated from duplicates and reported in table 2. This error is assigned as an analytical error, reflecting IC-PMS precision, not deviation from duplicate averages. Published basalt data reflects the isotopic diversity of mantle derived basalts, probably reflecting recycling of oceanic crust (Nielsen et al., 2007). “Typical” mantle-derived basalt values (average MORB) are thought to be about  $-1.9 \pm 0.6$  (Nielsen et al., 2006).

### 5.2.1 Sourcing Paleozoic Sedimentary Host Rocks

Emsbo et al. (2003) proposed that CTDs may have sourced metals from the Devonian host rocks at the Meikle CTD, particularly from interpreted exhalative sulfide-rich

horizons within the Devonian stratigraphic sections. Gold (and presumably Tl) in this enriched source is postulated by Emsbo et al (2003) to have been remobilized in the Eocene by later hydrothermal fluids of meteoric origin, which locally redistributed gold along faults and adjacent carbonate strata in what is now the Meikle CTD.

In a similar model to Emsbo et al.'s (2003) model, Large et al. (2011) also proposed that metal accumulations above background, particularly in respect to Au and As, occurred during deposition of host sediments. Their model called for the formation of diagenetic arsenian pyrite that formed in carbonaceous slope facies that host Carlin-type mineralization at Meikle and other deposits in the northern Carlin trend. The study presented LA-ICP-MS analyses of these pyrites which showed elevated Au and Tl as well as other metals that comprise the geochemical signature of CTDs (As, Sb, Hg). The model suggested that elevated metal concentrations were due to extraction from seawater and marine clays during sedimentation and diagenesis. They proposed that these metal-enriched diagenetic arsenian pyrite grains were the source of metals observed in CTDs. They argued that later greenschist facies metamorphism and conversion of these pyrite to pyrrohotite would have released metals, and, like Emsbo et al.'s (2003) model, would have remobilized metals in fluids that deposited the metals along high-angle faults and adjacent carbonate rocks (Large et al., 2011).

A point of contention with the model proposed by Large et al. (2011) is that host pyrite (cores of ore pyrite) in CTDs are not elevated in As relative to background values (fig. 5) and the study did not present evidence of the hypothesized deep pyrrohotite which would have released, in its formation, the metals responsible for CTDs. Furthermore, evidence for

shallow metamorphism into the greenschist facies in the Devonian sedimentary sequence in the northern Carlin trend is lacking.

Our data does not indicate Paleozoic carbonate rocks as a likely source of metals in CTDs. The enriched arsenian pyrite described above does contain the geochemical suite observed in CTDs. However, the metal suite is hypothesized to have been sourced directly from seawater, which is inconsistent with the Tl isotope data presented here. Average seawater Tl values are isotopically much lighter than the values for ore- and late-stage Carlin mineralization.

### 5.2.2 Sourcing Metamorphosed Neoproterozoic Clastic Rocks

Seedorff (1991) proposed a source of metals from the metamorphosed Neoproterozoic clastic wedge. The model suggest that metals may have been released by (1) crustal heating induced by the voluminous magmatism in the Eocene, where a metamorphic fluid was generated by dehydration reactions during metamorphism, (2) an older metalliferous, metamorphic fluid, trapped for tens of millions of years, may have been mobilized at the onset of extension, or (3) that deep circulating meteoric fluid may have leached metals from the clastic wedge.

The later scenario (3) was addressed in further detail by Ilchik and Barton (1997). They investigated the proposition that deeply circulating meteoric fluids, heated by rapid crustal extension, could have leached metals from the late Proterozoic metasedimentary clastic wedge underling the Paleozoic carbonate rocks that host the CTDs by performing geochemical modeling. Conditions for the model began at 1 kbar and 300°C and where brought up to 0.5 kbar and 225° to 150°C, simulating the ascension and cooling of the fluids

from the brittle-ductile transition zone to the depth of deposition. Unlike Large et al. (2011), however, Ilchik and Barton (1997) did not propose a pre-enriched source. Instead, their geochemical modeling indicated a potential source for Au could have been arkosic sandstones, present as a protolith in the late Proterozoic to early Cambrian metasedimentary sequence underlying the Great Basin. This arkosic sandstone is represented in our sample suite by samples McCoy 1 and McCoy 3, quartzites from the Neoproterozoic clastic wedge.

Our data shows an excellent correlation with most of the late Proterozoic to early Cambrian metasedimentary rocks (in fig. 9 labeled “Proterozoic Clastic Metasediments”) and the ore-stage sample. The exception is sample McCoy 5, a significantly weathered phyllite, which does show a moderate correlation with the late stage sample. The metamorphosed clastic wedge, therefore, is an excellent candidate for a metalliferous source of Carlin-type deposits.

### 5.2.3 Sourcing Magmatic Products

Muntean et al. (2011) proposed a model which described the formation of magma from the enriched mantle wedge during slab roll back, which would have released a metalliferous aqueous fluid in the crust. They proposed that the fluid underwent later phase separation, into a brine and vapor, during ascension. The phase separation would have been responsible for generating an evolved fluid consistent with CTDs; a fluid with relatively low salinity and the unique metal suite observed. The evolved ore fluid would have undergone significant mixing with shallow circulating meteoric water as it traveled up through the deep-seated normal faults accommodating extension, altering the isotopic signature of the ore fluid(s) from magmatic to the signature observed from many deposits which, while not truly

meteoric, resembles a signature consistent with evolved meteoric waters (Cline et al., 2005).

Our data shows an excellent correlation between the ore-stage and the mantle-analogous basalt sample; however data for Eocene extrusive and Mesozoic intrusive rocks correlate better with the late-stage sample. The fact that values for these samples are lighter than ore-stage values may indicate crustal assimilation during emplacement. As the Paleozoic carbonate rock values are significantly lighter, assimilation of these or similar rocks could account for this observation. Because the basalt sample had undergone little assimilation and short crustal residence, we believe that this value is representative of the mantle underlying the Great Basin.

### 5.3 Ore- to Late-Stage Isotopic Shift

The observed shift in Tl isotopic values from heavier ore-stage to lighter late-stage could be attributed to (1) mixing of the metamorphic/deep meteoric or magmatic ore fluid with shallow meteoric water interacting with, and over time leaching some Tl from, the Paleozoic sedimentary sequence or (2) isotopic fractionation of a deep fluid as the mineralizing system collapsed. The latter is unlikely as Tl fractionation does not readily occur though, as this isotopic system is still in the early stages of our understanding, cannot be ruled out. The former is more likely as sulfur and oxygen and deuterium data also support a model involving some meteoric fluid component which provides variable concentrations of sulfur leached from Paleozoic sedimentary rocks. Additionally, as the difference in isotopic signatures between the lightest Paleozoic carbonate sample and the ore-stage sample is so pronounced, little sedimentary Tl would be required to depress the ore-stage value to arrive at the value of the late-stage sample. Another explanation of the shift from ore- to late-stage

is simply that values fall within reasonable natural variation; as our analyses were limited, so are our resulting data. This explanation may also serve to expound the isotopic difference between our mantle and Eocene volcanic samples, as opposed to our interpretation of crustal assimilation. More data, specifically more data from a variety of deposits in northern Nevada, may place further constraints on the sources of Tl and, thus, Au.

## 6. Conclusions

Although not pointing to an unequivocal source for the Tl (and by proxy Au), the Tl isotope data appear to rule out early Paleozoic passive margin carbonate rocks as a metal source for ore-stage deposition. Comparison of ore- to late- stage minerals may suggest a shift in Tl isotope compositions that is consistent with mixing of the ore-stage fluid with meteoric fluids. While higher values of ore-stage mineralization correlate well with a source from the Neoproterozoic clastic wedge or a mantle-derived magmatic Au source, isotopic values are lighter for late-stage mineralization consistent with what would be expected for system mixing with an isotopically lighter metal source. This source would likely have been upper crustal Paleozoic sedimentary sequence as less Tl would need to be sourced from these rocks, compared to Eocene and Mesozoic igneous rocks, to shift the isotopic signature of the ore-stage sample to the lighter isotopic values observed from the late ore-stage sample. We propose that this evidence supports deeply sourced Tl and Au from either a mantle-derived magmas or Neoproterozoic clastic rocks, which interacted with an evolved meteoric fluid containing isotopically lighter Tl but no significant concentrations of Au.

## References

- Arehart, G. B. (1996). Characteristics and origin of sediment-hosted disseminated gold deposits: a review. *Ore Geology Reviews*, *11*, 383-403.
- Arehart GB, Chakurian AM, Tretbar DR, Christensen JN, McInnes BA, Donelick RA (2003) Evaluation of radioisotope dating of Carlin-type deposits in the Great Basin, western North America, and implication for deposit genesis. *Economic Geology*, *98*, 235–248.
- Arehart, G.B., Chryssoulis, S.L., and Kesler, S.E. (1993). Gold and arsenic in iron sulfides from sediment-hosted disseminated gold deposits; implications for depositional processes. *Economic Geology*, *88*, 171-185.
- Arehart, G.B., DeYoung, S., Poulson, S.R., Heaton, J.S., and Weiss, S. (2013). Sulfur isotopes in plutonic rocks of the Great Basin as indicators of crustal architecture. *Journal of Geology*, *121* (4), 355-369.
- Baker, R. G. A., Rehkämper, M., Ihlenfeld, C., Oates, C. J., & Coggon, R. (2010). Thallium isotope variations in an ore-bearing continental igneous setting: Collahuasi formation, northern Chile. *Geochimica et Cosmochimica Acta*, *74*(2010), 4405-4416.
- Bakken, B.M., Hochella, M.F., Marshall, A.F., & Turner, A.M. (1989). High-resolution microscopy of gold in the unoxidized ore from the Carlin Mine, Nevada. *Economic Geology*, *84*, 171-179.
- Barker, S. L., Hickey, K.A., Cline, J.S., Dipple, G.M., Kilburn, M.R., Vaughan, J.R., and Longo, A. A. (2009). Uncloaking invisible gold: Use of nanoSIMS to evaluate gold,

- trace elements and sulfur isotopes in pyrite from Carlin-type gold deposits. *Economic Geology*, 104, 897–904.
- Bigeleisen, J. (1996). Nuclear size and shape effects in chemical reactions. Isotope chemistry of the heavy elements. *J. Am. Chem. Soc.*, 118(15), 3676–3680.
- Bigeleisen J. and Mayer M.G. (1947) Calculation of equilibrium constants for isotopic exchange reactions. *J.Chem. Phys.* 15, 261-267.
- Blondes, M. S., Reiners, P. W., Ducea, M. N., Singer, B. S., & Chesley, J. (2008). Temporal–compositional trends over short and long time-scales in basalts of the Big Pine Volcanic Field, California. *Earth and Planetary Science Letters*, 269, 140-154.
- Cail, T. L., & Cline, J. S. (2001). Alteration associated with gold deposition at the Getchell Carlin-type gold deposit, north-central Nevada. *Economic Geology*, 96, 1343-1359.
- Chevillon, V., Berentsen, E., Gingrich, M., Howla, D.B., and Zbinden, E. (2000). Geological overview of the Getchell gold mine geology, exploration, and ore deposits, Humboldt County, Nevada. Geology and gold deposits of the Getchell Trend: *Society of Economic Geologists Guidebook Series*, 32, p. 195–201.
- Cassinero, M. D. and Muntean, J. L. (2011). Patterns of lithology, structure, alteration and trace elements around high-grade ore zones at the Turquoise Ridge gold deposit, Getchell district, Nevada: *in* Steininger, R. C. and Pennell, W. M. (eds.), Great Basin Evolution and Metallogeny: Geological Society of Nevada 2010 Symposium Proceedings, Reno, p. 949-978.

- Cline, J.S. (2001). Timing of gold and arsenic sulfide mineral deposition at the Getchell Carlin-type gold deposit, north-central Nevada: *Economic Geology*, 96, p. 75–89
- Cline, J. S., Hofstra, A. H., Muntean, J. L., Tosdal, R. M., & Hickey, K. A. (2005). Carlin-type gold deposits in Nevada: Critical geological characteristics and viable models. *Society of Economic Geologists: Economic Geology 100th Anniversary Volume*, 451-484.
- Cline, J.S., & Hofstra, A.A. (2000). Ore-fluid evolution at the Getchell Carlin-type gold deposit, Nevada, USA. *European Journal of Mineralogy*, 12, 195-212.
- Cline, J.S., Muntean, J.L., Longo, A.A., and Cassinero, M.D. (2008). Collaborative Research on Fluid Pathways and Metal Transport in Carlin-type Gold Deposits: Insights from the Getchell deposit. Final Report for the U.S. Geological Survey 2006 Mineral Resources External Research Program.
- Coney, P.J., & Harms, T.A. (1984). Cordilleran metamorphic core complexes: Cenozoic extensional relicts of Mesozoic compression. *Geology*, 12, 550-554.
- Dickinson, W. R. (2004). Evolution of the North American cordillera. *Annu. Rev. Earth Planet. Sci.*, 32, 13-45.
- Dickinson, W. R. (2006). Geotectonic evolution of the Great Basin. *Geosphere*, 2(7), 353-368.
- Dobosz, A.N. (2012). Characterization of Carlin-type auriferous arsenian pyrite from the Goldstrike property using EMP, SIMS, and Vespers Synchrotron  $\mu$ -XRF: Constraints to ore deposition mechanisms. (Unpublished Masters thesis). Queen's University, Kingston, Ontario, Canada.

- Emsbo, P., Groves, D.I., and Hofstra, A. H. (2006). The giant Carlin gold province: a protracted interplay of orogenic, basinal, and hydrothermal processes above a lithospheric boundary. *Miner Deposita*, 41, 517-525.
- Emsbo, P., Hofstra, A. H., Lauha, E. A., Griffin, G. L., & Hutchinson, R. W. (2003). Origin of high-grade gold ore, source of ore fluid components, and genesis of the Meikle and neighboring Carlin-type deposits, northern Carlin trend, Nevada. *Economic Geology and the Bulletin of the Society of Economic Geologists*, 98(6), 1069-1105.
- Fujii Y, Nomura M, Onitsuka H et al (1989) Anomalous isotope fractionation in uranium enrichment process. *J Nucl Sci Technol*, 26(11): 1061–1064.
- Groff, J.A., Heizler, M.T., McIntosh, W.C., and Norman, D.I., 1997,  $^{40}\text{Ar}/^{39}\text{Ar}$  dating and mineral paragenesis for Carlin-type gold deposits along the Getchell trend: Evidence for Cretaceous and Tertiary gold mineralization. *Economic Geology*, 92, 601–622.
- Hall C.M., Kesler S.E., Simon G., Fortuna J. (2000) Overlapping Cretaceous and Eocene alteration, Twin Creeks Carlin-type deposit, Nevada. *Economic Geology*, 95, 1739–1752
- Hoefs, J. (1997). Stable isotope geochemistry. Berlin: Springer-Verlag.
- Hofstra, A.H., and Cline, J.S. (2000). Characteristics and models for Carlin-type gold deposits. *SEG Reviews*, 13, 163-220.
- Humphreys, E. (1995). Post-Laramide removal of the Farallon slab, western United States. *Geology*, 23(11), 987–990.
- Ilchik, R.P., & Barton, M. D. (1997). An amagmatic origin of Carlin-type gold deposits. *Economic Geology*, 92, 269-288.

- John, D.A., Henry, C.D., and Colgan, J.P. (2008). Magmatic and tectonic evolution of the Caetano caldera, north-central Nevada: A tilted, mid-Tertiary eruptive center and source of the Caetano Tuff. *Geosphere*, 4(1), 75-106.
- Kesler, S.E., Riciputi, L.C., & Zaojun, Y. (2005). Evidence for a magmatic origin for Carlin-type gold deposits: Isotopic composition of sulfur in the Betze-Post-Screamer Deposit, Nevada, USA. *Mineralium Deposita*, 40(2), 127-136.
- Large, R., Bull, S., & Maslennikov, V. V. (2011). A carbonaceous sedimentary source-rock model for Carlin-type and orogenic gold deposits. *Economic Geology*, 106, 331-358.
- May, W. E., & Watters, R. L. (2004). National Institute of Standards & Technology Certificate of Analysis Standard Reference Material 997 Isotopic Standard for Thallium. Retrieved May 1, 2014, from <https://www-s.nist.gov/srmors/certificates/997.pdf?CFID=3063044&CFTOKEN=b337c2b3dc99042-B9B600B0-0F41-350C-782CA75F6BEA1168&jsessionid=f03098cab791ce35771f45541e583e207913>
- Misch, P., & Hazzard, J. C. (1962). Stratigraphy and metamorphism of late Precambrian rocks in central northeastern Nevada and adjacent Utah. *Association of Petroleum Geologists*.
- Muntean, J. L., Cline, J. S., Simon, A. C., & Longo, A. A. (2011). Magmatic–hydrothermal origin of Nevada’s Carlin-type gold deposits. *Nature Geoscience*, 4, 121-127.
- Muntean, J. L., Cassinerio, M. D., Arehart, G. B. Cline, J. S., and Longo, A. A., (2009). Fluid pathways at the Turquoise Ridge Carlin-type gold deposit, Getchell district,

Nevada: *in* Williams, P. J. (ed.), *Smart Science for Exploration and Mining*, Proceedings of the Tenth Biennial Meeting of the Society for Geology Applied to Mineral Deposits, Townsville, Australia, p. 251-253.

Muntean, J. L., Coward, M. P., & Tarnocai, C. A. (2007). Reactivated Palaeozoic normal faults: controls on the formation of Carlin-type gold deposits in north-central Nevada. In A. Ries, R. Butler & R. Graham (Eds.), *Deformation of the Continental Crust: The Legacy of Mike Coward* (272 ed., pp. 571-587). London: Geological Society of London.

Nielsen, S. G., Rehkämper, M., Teagle, D. A. H., Butterfield, D. A., Alt, J. C., & Halliday, A. N. (2006). Hydrothermal fluid fluxes calculated from the isotopic mass balance of thallium in the ocean crust. *Earth and Planetary Science Letters*, 251, 120-133.

Nielsen, S. G., Rehkämper, Brandon, A.D., Norman, M.D, Turner, S., & O'Reilly, S.Y. (2007). Thallium isotopes in Iceland and Azores lavas- Implications for the role of altered crust and mantle geochemistry. *Earth and Planetary Science Letters*, 264(1-2), 332-345.

Nielsen, S. G., & Rehkämper, M. (2011). Thallium isotopes and their application to problems in earth and environmental science. In M. Baskaran (Ed.), *Handbook of Environmental Isotope Geochemistry* Berlin, Heidelberg: Springer-Verlag.

Nriagu, J. O. (1998). *Thallium in the environment*. New York: Wiley.

- O'Driscoll, L.J., Humphreys, E.D., & Saucier, F. (2009). Subduction adjacent to deep continental roots: Enhanced negative pressure in the mantle wedge, mountain building and continental motion. *Earth and Planetary Science Letters*, 280(1-4), 61-70.
- Patterson, L. M. and Muntean, J. L., 2011, Multi-element geochemistry across a Carlin-type gold district: Jerritt Canyon, Nevada: *in* Steininger, R. C. and Pennell, W. M. (eds.), Great Basin Evolution and Metallogeny: Geological Society of Nevada 2010 Symposium Proceedings, Reno, p. 1119-1152.
- Person, M., Banerjee, A., Hofstra, A., Sweetkind, D., & Gao, Y. (2008). Hydrologic models of modern and fossil geothermal systems in the great basin: Genetic implications for epithermal Au-Ag and carlin-type gold deposits. *Geosphere*, 4(5), 888-917.
- Rehkämper M., & Halliday A.N. (1999). The precise measurement of Tl isotopic compositions by MC- ICPMS: application to the analysis of geological materials and meteorites. *Geochimica et Cosmochimica Acta*, 63, 935–944.
- Rehkämper, M., Frank, M., Hein, J. R., Porcelli, D., Halliday, A., Ingri, J., & Liebetrau, V. (2002). Thallium isotope variations in seawater and hydrogenetic, diagenetic, and hydrothermal ferromanganese deposits. *Earth and Planetary Science Letters*, 197(1-2), 65-81.
- Ressel, M.W., and Henry, C.D. (2006). Igneous geology of the Carlin trend, Nevada: Development of the Eocene plutonic complex and significance for Carlin-type gold deposits. *Economic Geology*, 101, 347-383.

- Schauble, E. A. (2007). Role of nuclear volume in driving equilibrium stable isotope fractionation of mercury, thallium, and other very heavy elements. *Geochimica et Cosmochimica Acta*, 71, 2170-2189.
- Stenger, D.P., Kesler, S.E., Peltonen, D.R., and Trapper, C.J. (1998). Deposition of gold in Carlin-type deposits: The role of sulfidation and decarbonation at Twin Creeks, Nevada. *Economic Geology*, 93, 201-215.
- Tretbar, D. R., Arehart, G. B., & Christensen, J. N. (2000). Dating gold deposition in a Carlin-type gold deposit using Rb/Sr methods on the mineral galkhaite. *Geology*, 28(10), 947-950.
- Trexler, J. H., Cashman, P. H., Cole, J. C., Snyder, W. S., Tosdal, R. M., & Davydov, V. I. (2003). Widespread effects of middle Mississippian deformation in the Great Basin of Western North America. *Geological Society of America Bulletin*, 11(10), 1278-1288.
- Wells, J.D., & Mullens, T.E. (1973). Gold-bearing arsenian pyrite determined by microprobe analysis, Cortez and Carlin Gold Mines, Nevada. *Economic Geology*, 68, 187-201.
- White, W. M. (2013). *Geochemistry*. Wiley-Blackwell.

**Appendix:**

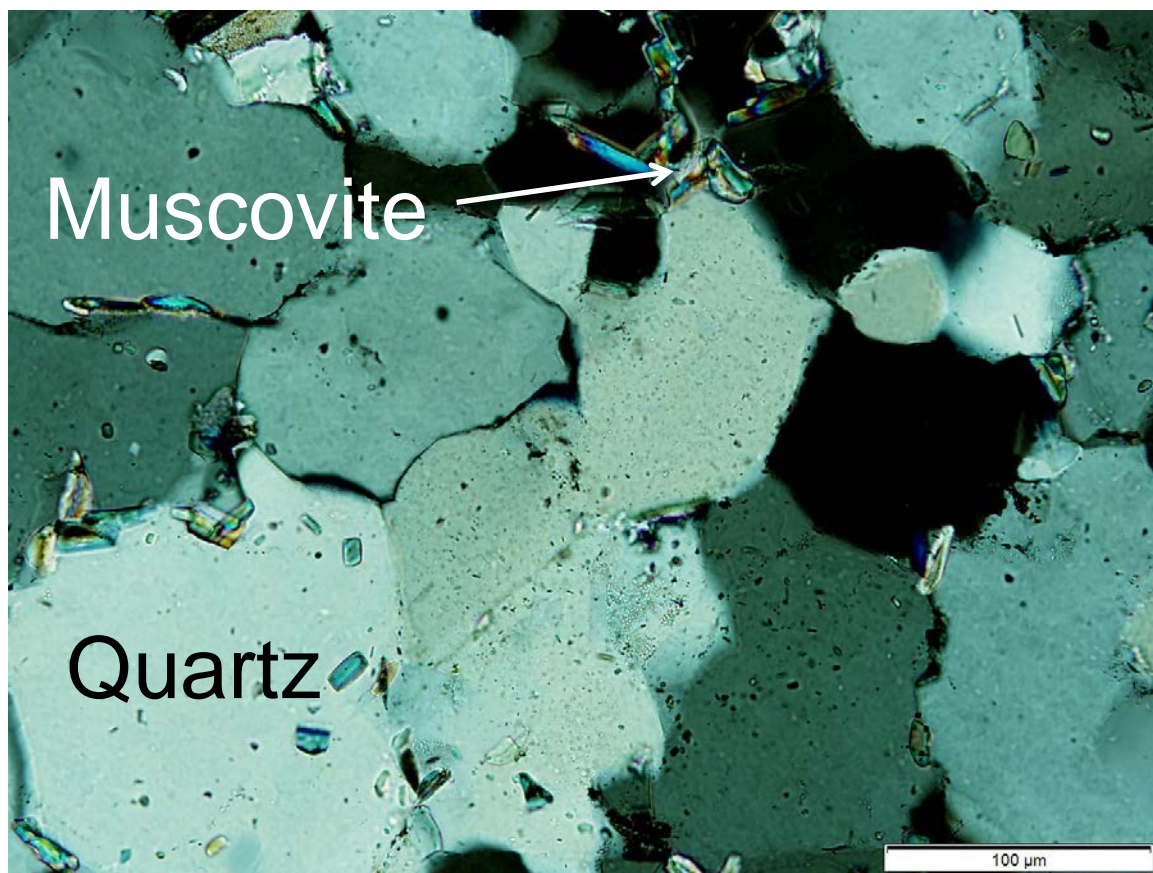
Thin Section Characterization of Samples

## A1 McCoy Creek Quartzites

Sample: McCoy 1

Rock type: Metasediment, Quartzite

$\epsilon^{205}\text{Tl}$ : -1.44

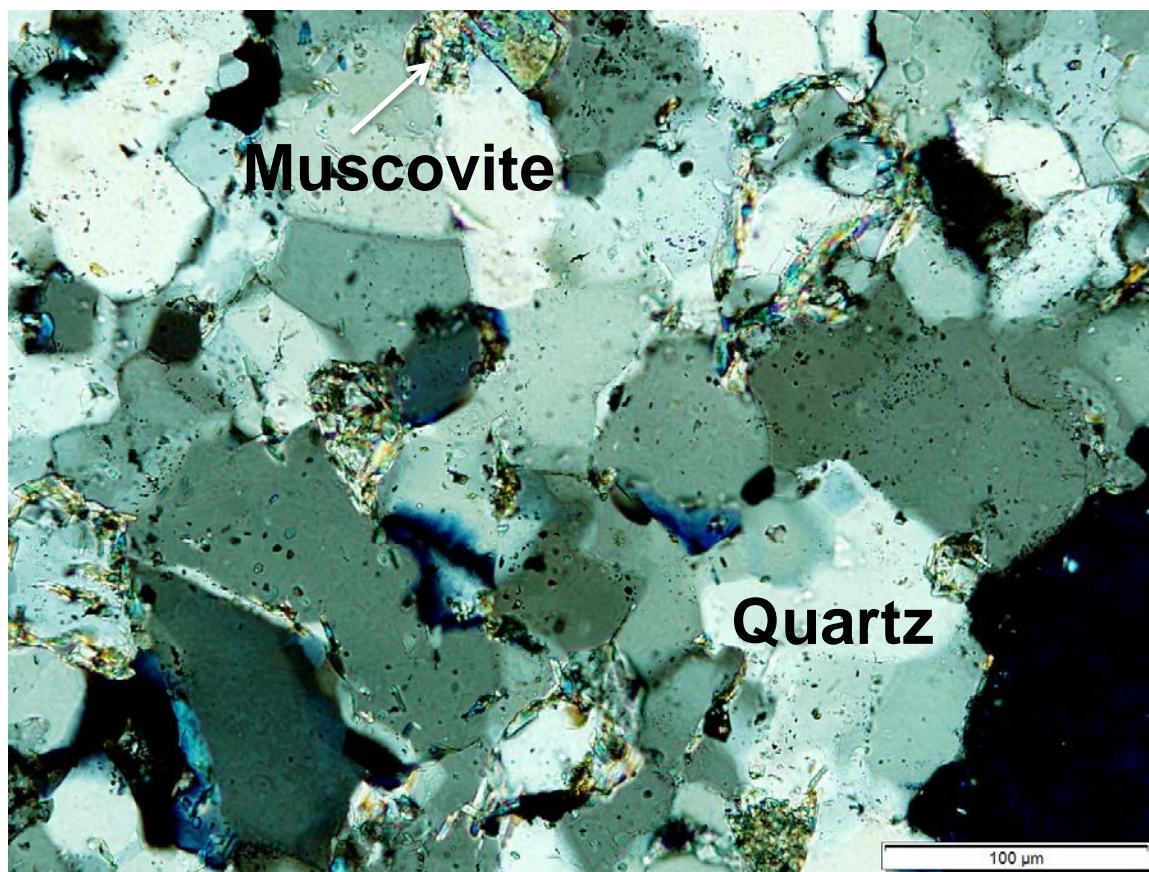


McCoy 1 contains approximately 97% quartz and 3% fine grained muscovite.

Sample: McCoy 3

Rock type: Metasediment, Quartzite

$\epsilon^{205}\text{Tl}$ : -1.58



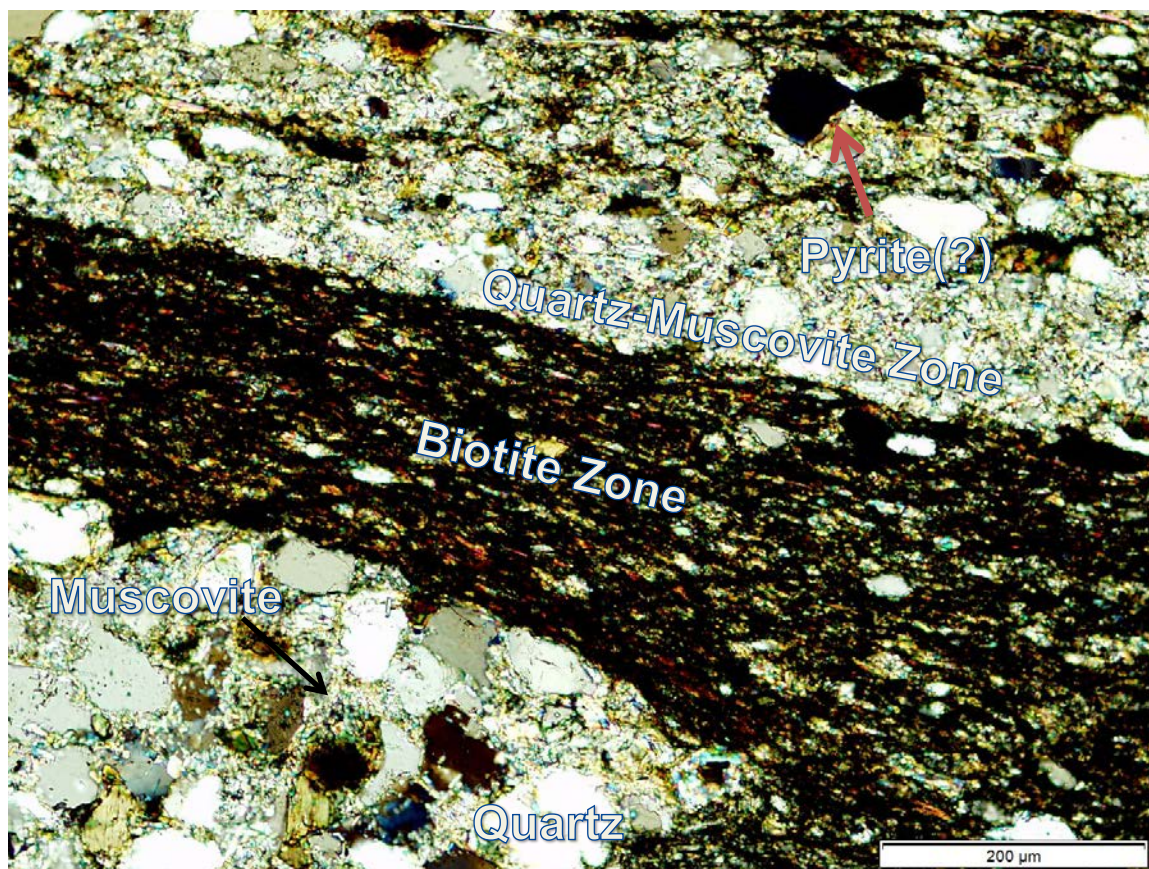
McCoy 3 contains approximately 95% quartz and 5% fine grained muscovite. Grains in McCoy 3 are more amoeboid in shape, compared to the equant boundaries seen in McCoy 1. Muscovite in McCoy 3 are similarly less well formed in regards to crystal shape. Quartz grains on average are also slightly smaller in McCoy 3 compared to McCoy 1.

## A2 McCoy Creek Phyllites

Sample: McCoy 4

Rock type: Metasediment, Phyllite

$\epsilon^{205}\text{Tl}$ : -1.54

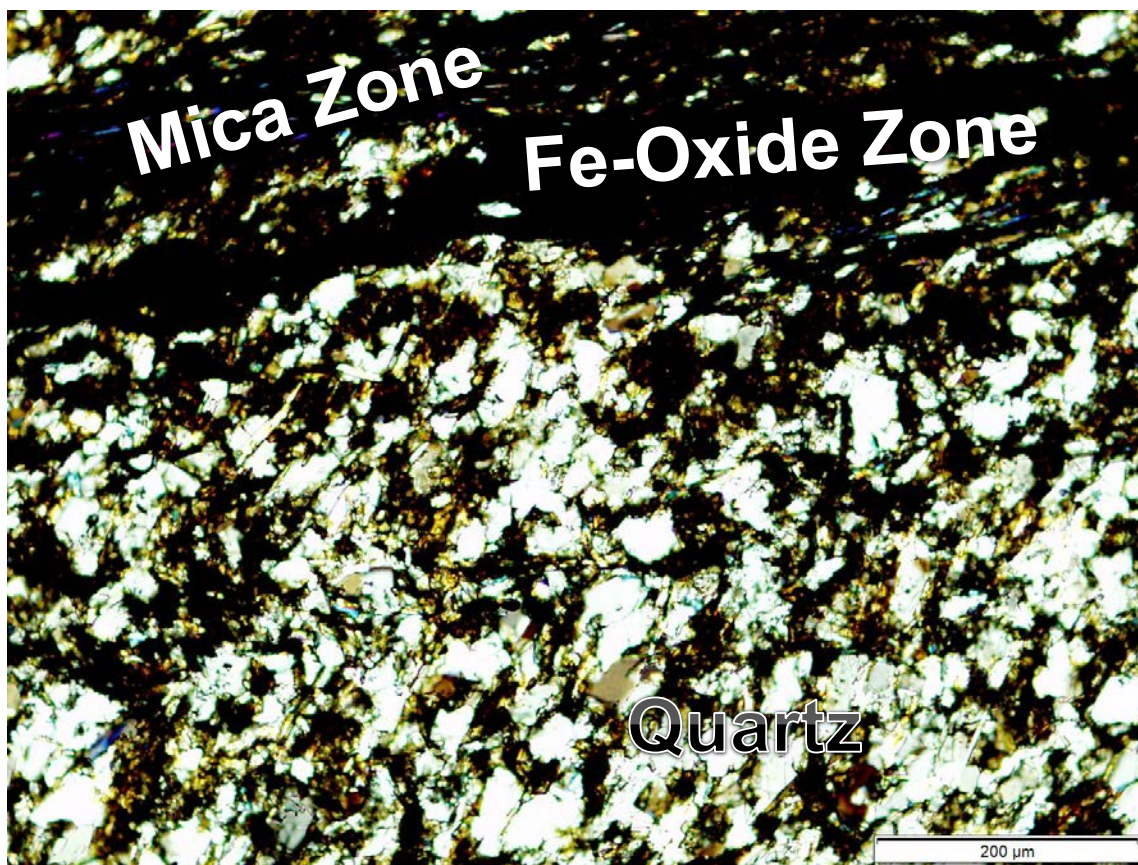


McCoy 4 is a foliated quartz mica phyllite. Major mineralogical phases include quartz, muscovite, and biotite. Not in the picture above distinct biotite zones containing minor quartz and muscovite and zones with larger grained quartz with muscovite occurring interstitially. Pyrite and goethite (after pyrite) were observed in reflected light petrography.

Sample: McCoy 5

Rock type: Metasediment, Phyllite

$\epsilon^{205}\text{Tl}$ : -2.41



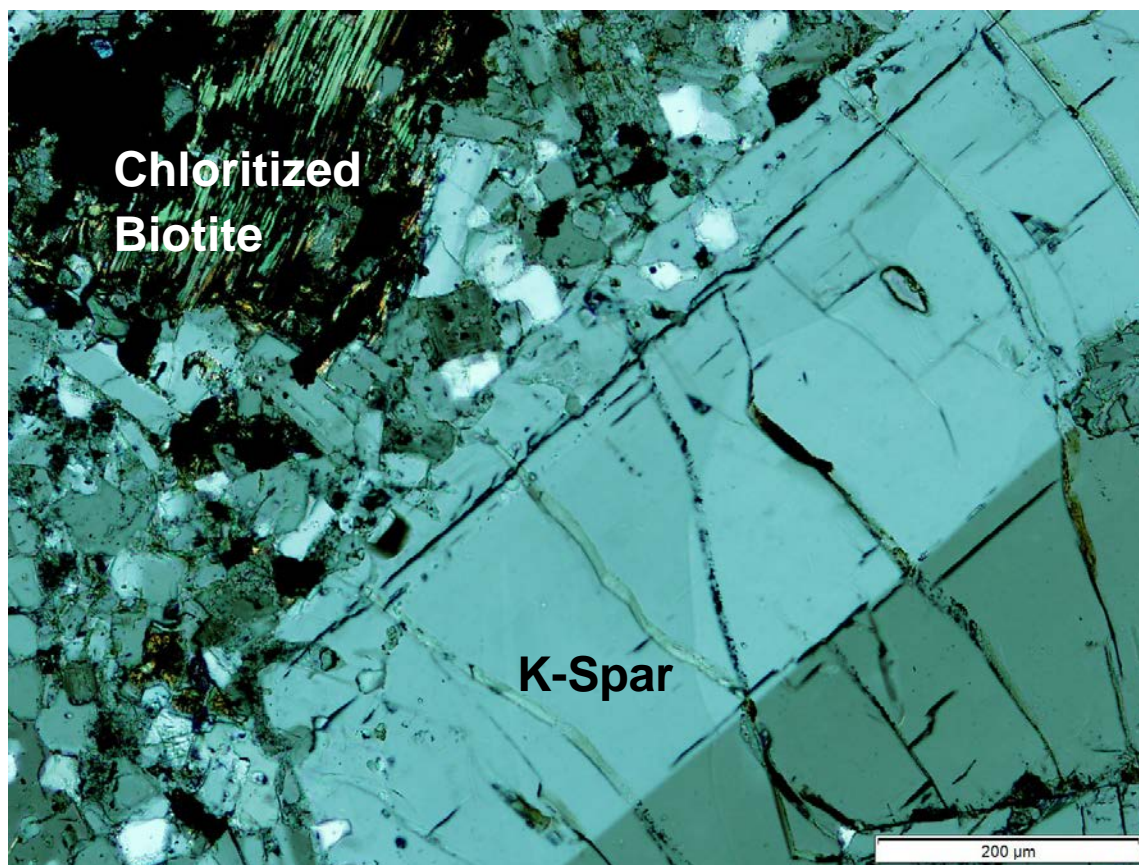
McCoy 5 has undergone significant iron oxidation related to weathering, observed as large red zones (strong hematite internal reflections). Primary mineralogy includes biotite, quartz, and muscovite. Cubic oxidized pits may indicate primary pyrite that has undergone significant weathering.

### A3 Caetano Tuff

Sample: Caetano 1

Rock type: Felsic Ash-flow Tuff

$\epsilon^{205}\text{Tl}$ : -1.95

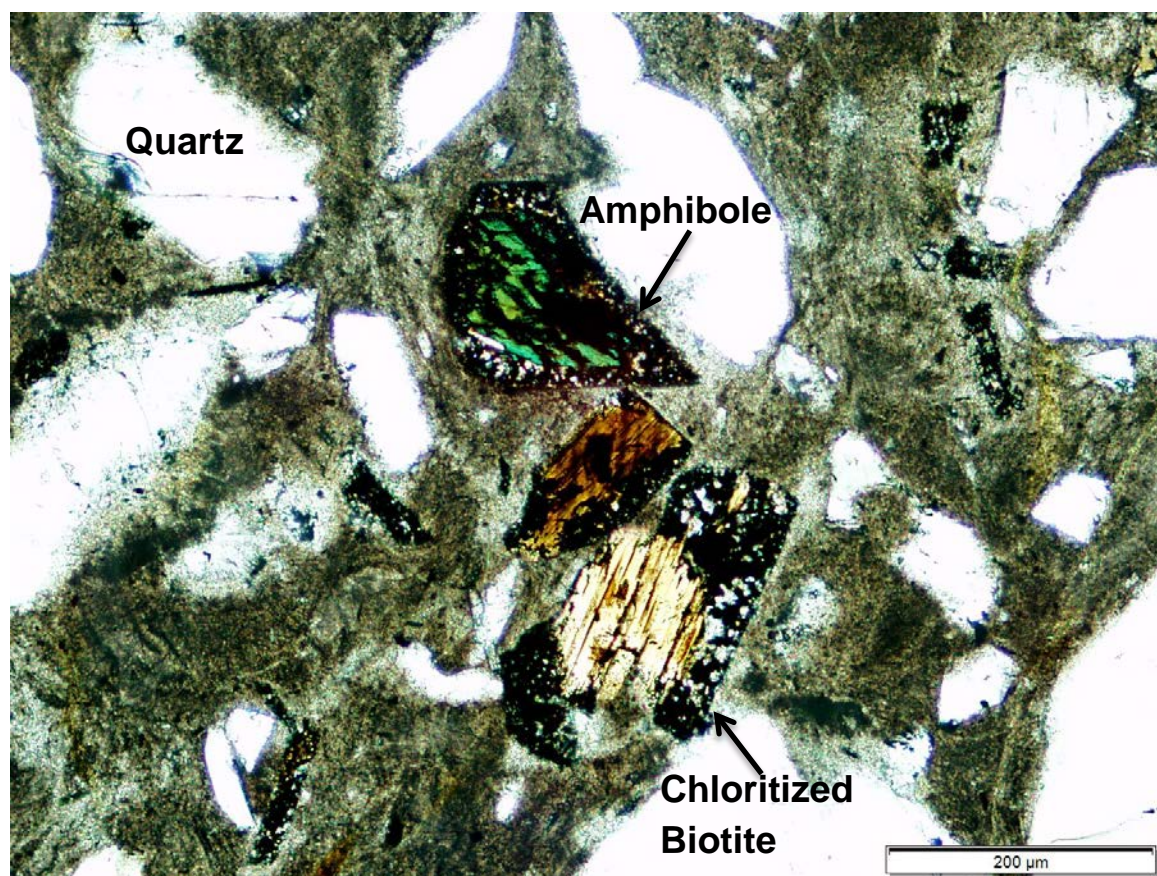


Caetano 1 displays porphyritic texture with feldspar and quartz grains comprising the groundmass. Phenocryst mineralogy includes potassium and plagioclase feldspars, quartz, and chloritized biotite.

Sample: Caetano 2

Rock type: Felsic Ash-flow Tuff

$\epsilon^{205}\text{Tl}$ : -2.10



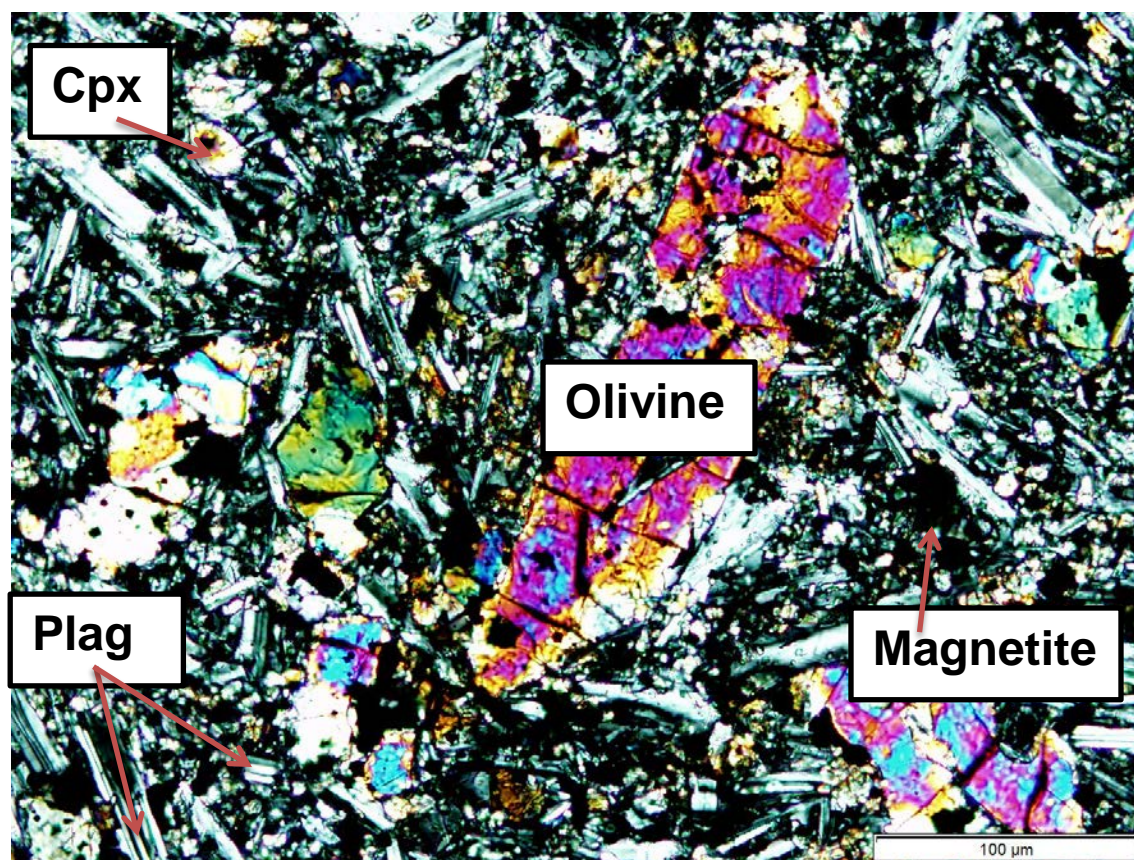
Caetano 2 has a finer grained groundmass than Caetano 1. The groundmass is dominated by glass, though small areas have a fine grained quartz groundmass. Phenocrysts are smaller on average than Caetano 1 and more mafics were present, including minor amphibole not observed in Caetano 1. Potassium feldspar is rarer in Caetano 2 than in Caetano 1.

## A4 Papoose Canyon Basalt

Sample: Papoose 2

Rock type: Olivine Basalt

$\epsilon^{205}\text{Tl}$ : -1.13



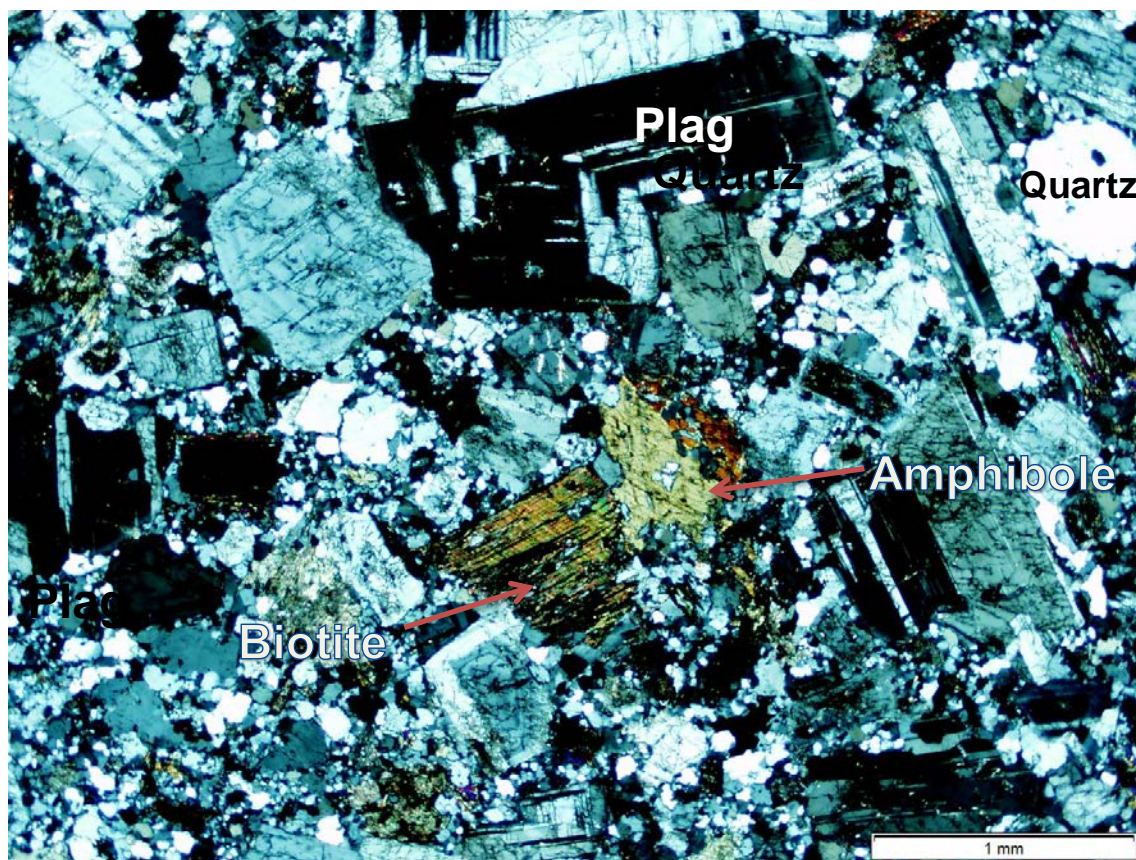
Phenocrysts of Papoose 2 are mainly olivine with minor orthopyroxene. Sample groundmass is comprised of swallow-tail plagioclase feldspar, fine grained clinopyroxene, and fine grained magnetite.

## A5 Mesozoic Intrusive

Sample: NM1164(26553)

Rock type: Granodiorite

$\epsilon^{205}\text{Tl}$ : -2.33



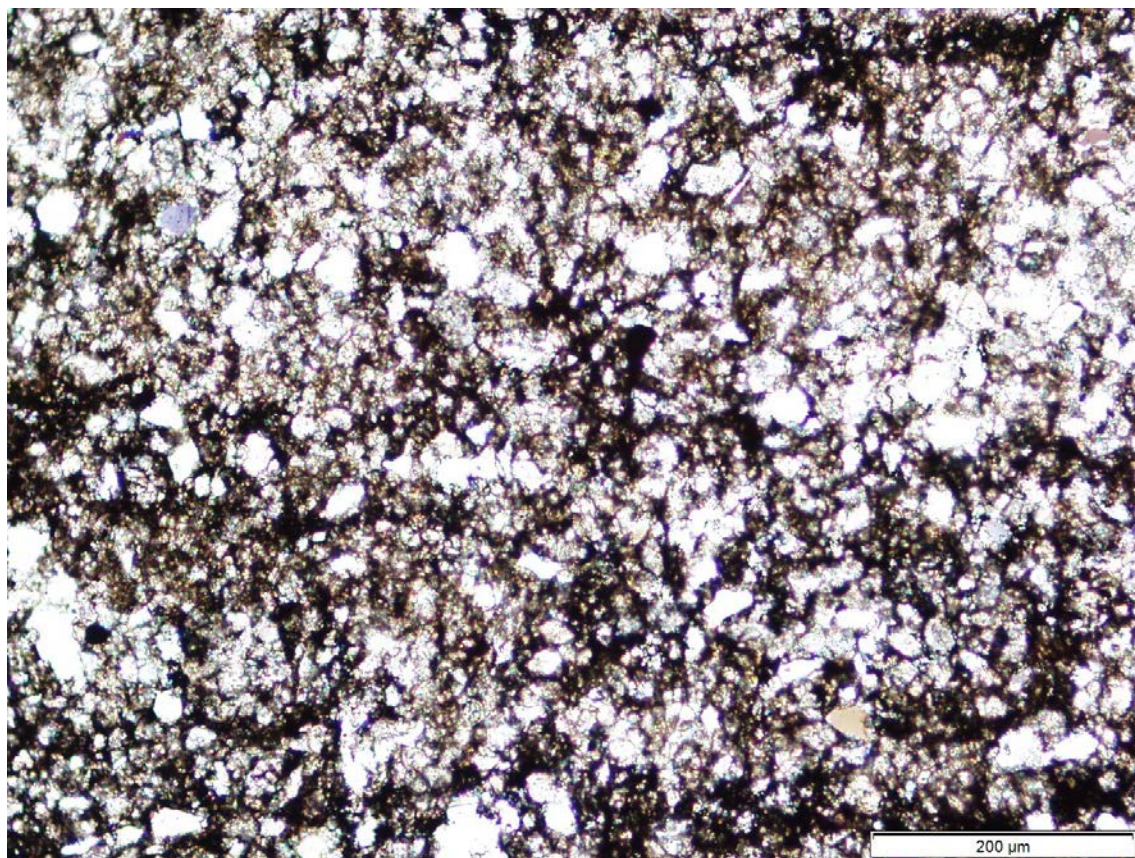
Sample NM1164(2653) has undergone mild alteration, evidenced by incomplete clay alteration of feldspar grains, minor chloritization of biotite, and presence of secondary pyrite (observed in reflected light). Major mineralogical phases include plagioclase feldspar, quartz, biotite, and amphibole.

## A6 Paleozoic Sedimentary Rocks

Sample: RMFJC020

Rock type: Calcareous Sandstone

$\epsilon^{205}\text{Tl}$ : -2.07

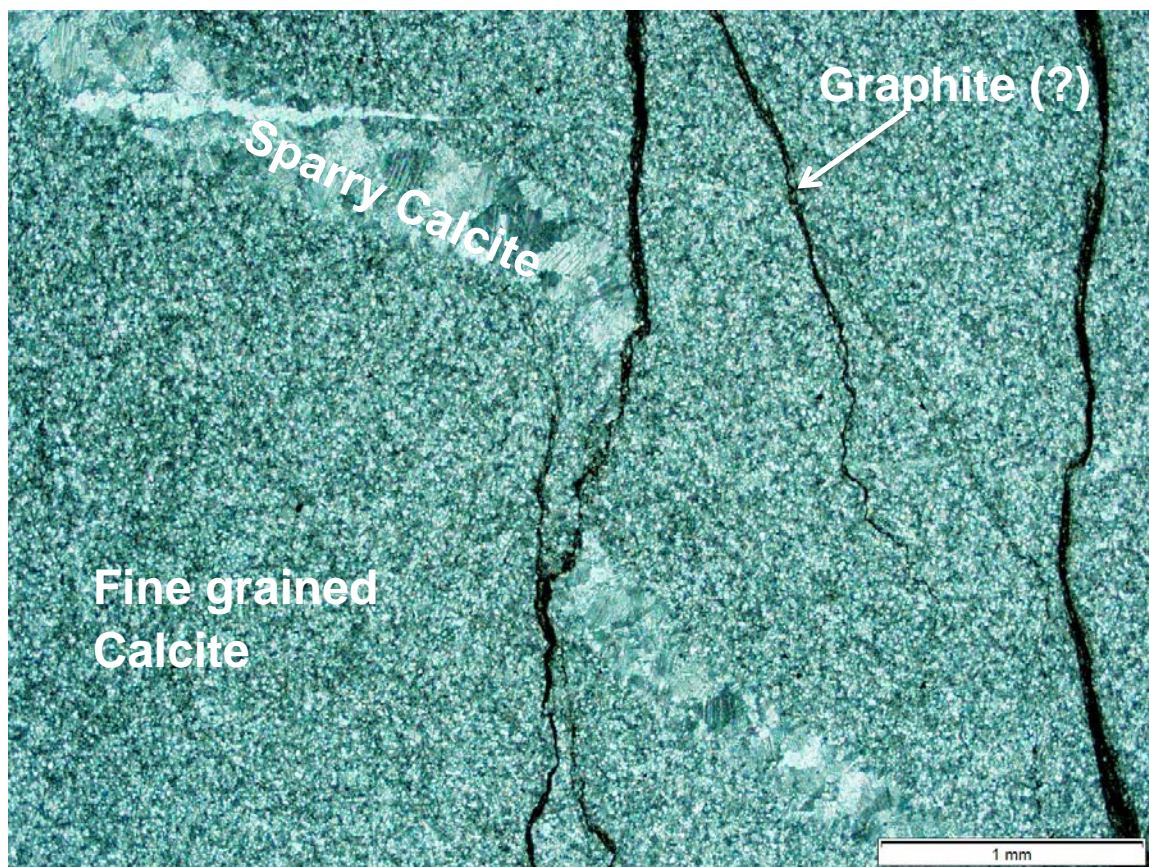


Sample RMFJC020 contains fine grained quartz and minor ( $\ll 1\%$ ) mica in a very fine grained groundmass which may be comprised of dolomite or siderite as it appears to have very high birefringence. Calcite is not likely as the sample was treated with HCl and was observed to be nearly non-reactive. Minor fine grained pyrite was observed in reflected light.

Sample: NM138

Rock type: Limestone

$e^{205}\Gamma$ : -2.72

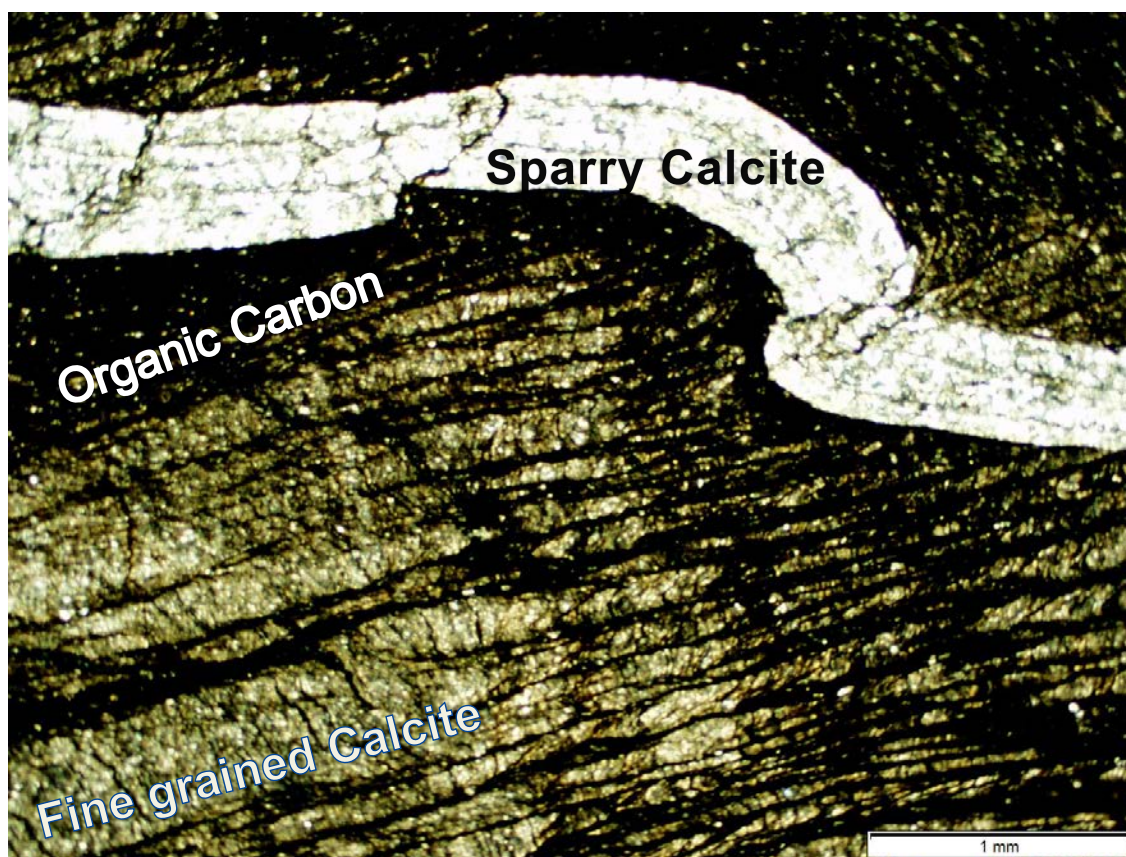


Sample is comprised of calcite which occurs as fine grained crystals with sparry calcite veinlets. Fine grained dark (graphite?) veinlets occur both cross cutting and being cut by the sparry calcite veinlets. Minor fine grained pyrite was observed in reflected light.

Sample: NM132

Rock type: Silty Limestone

$\epsilon^{205}\text{Tl}$ : -3.28



Sample is mainly comprised of fine grained calcite and organic carbon with abundant sparry calcite veinlets. Pyrite was observed in reflected light.